Freie Universität Berlin

HZB Helmholtz Zentrum Berlin

Frühjahrssitzung Arbeitskreis Energie der DPG, 16. – 17. 4. 2026, Bad Honnef

Susan Schorr

Research on emerging PV materials using large scale facilities

16. 4. 2026

Helmholtz-Zentrum Berlin für Materialien und Energie, Abteilung Struktur und Dynamik von Energiematerialien

Freie Universität Berlin, Institut für Geologische Wissenschaften

Forecast: energy mix until 2100

HZB Helmholtz Zentrum Berlin

Forecast of the Scientific Advisory Board of the German Government global environmental changes

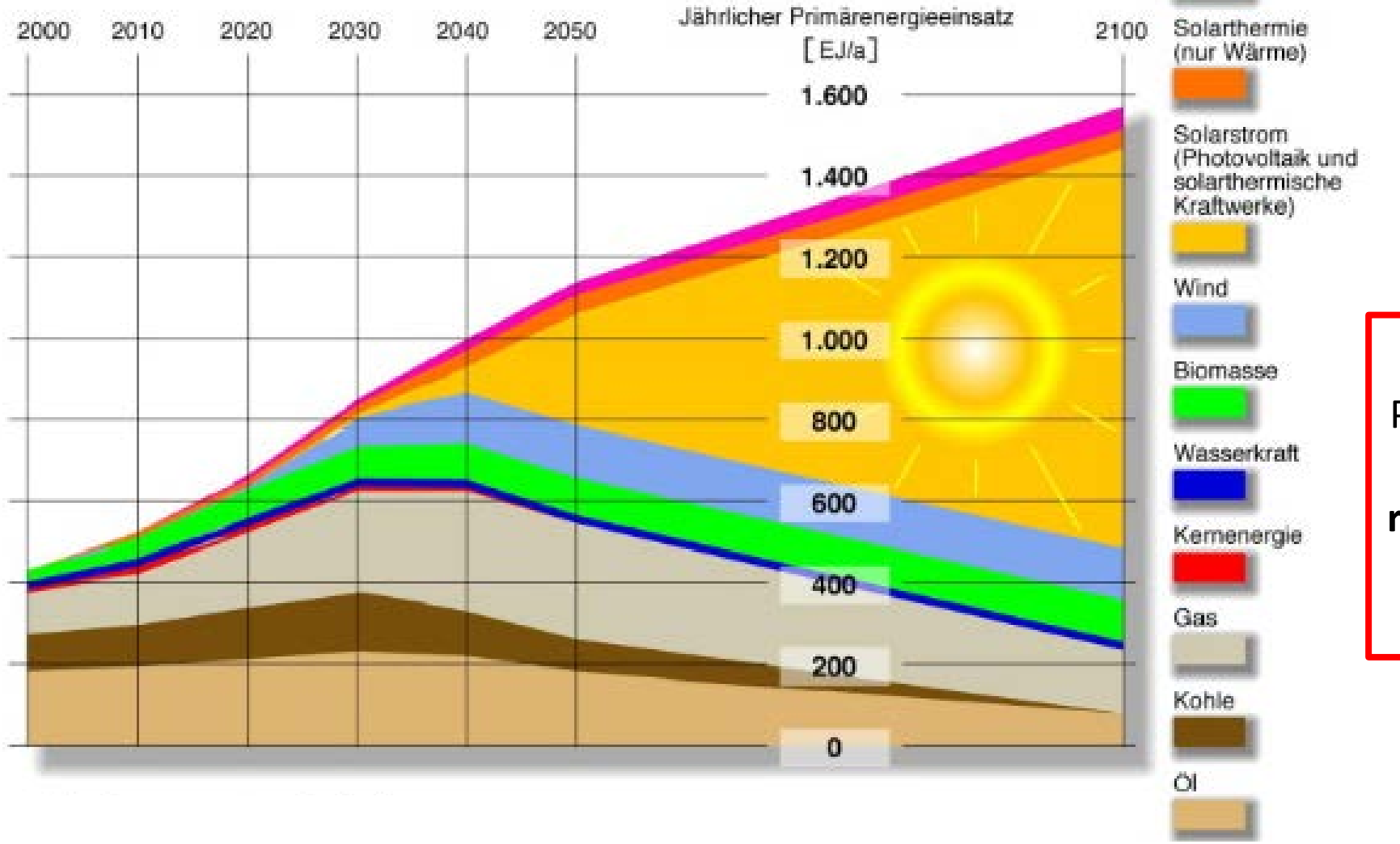

7 AFFORDABLE AND CLEAN ENERGY

SUSTAINABLE DEVELOPMENT GOALS

EU Energy Roadmap 2050

Photovoltaics (PV) is recognized as one of the main **renewable energy technologies** for the achievement of the defined targets

source: www.pv-leads.de

HZB Helmholtz Zentrum Berlin

Development of gross electricity production from renewable energy sources in Germany

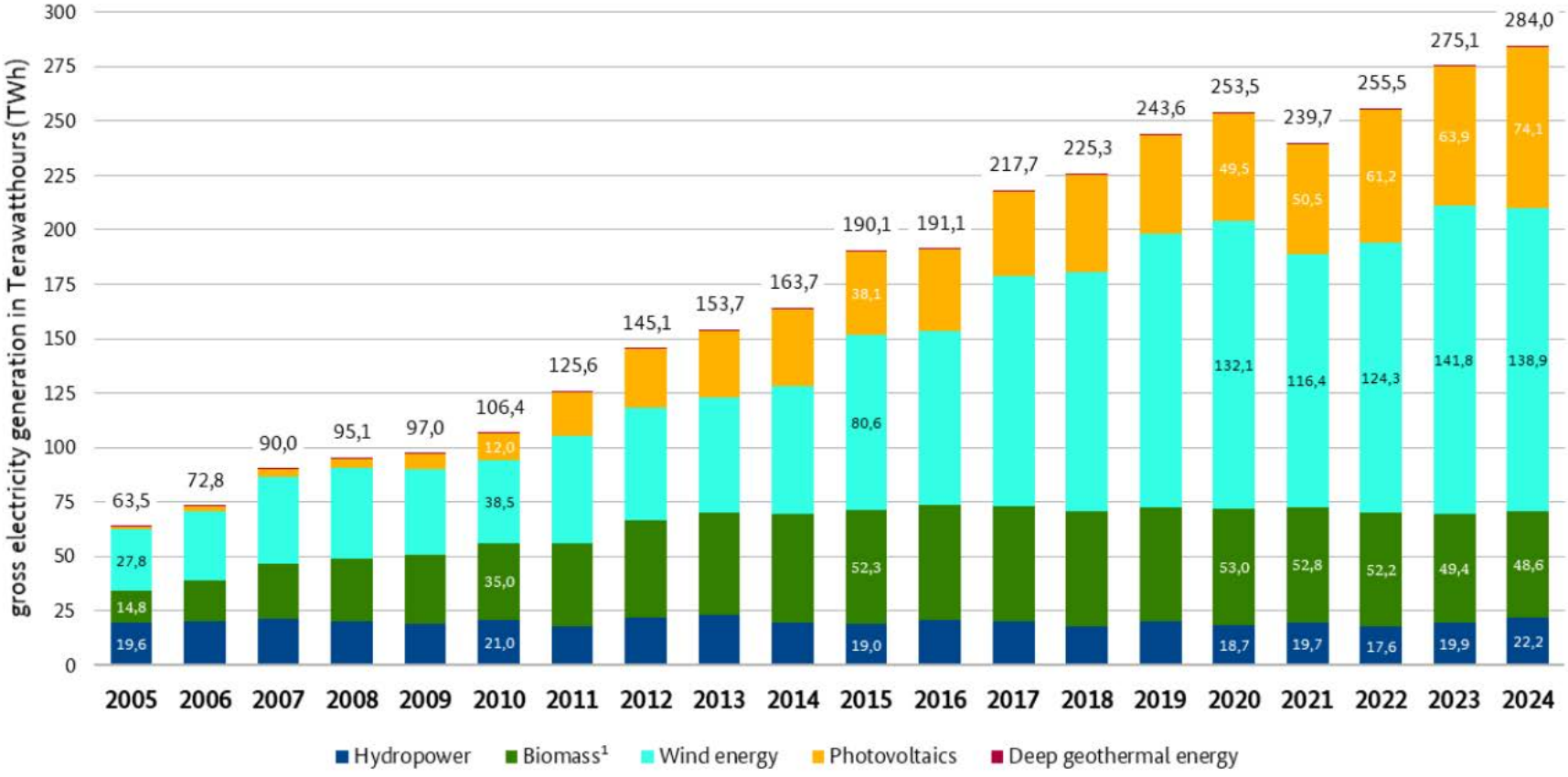

Source: BMWK, AGEE-Stat, Februar 2025

gross electricity production 2024

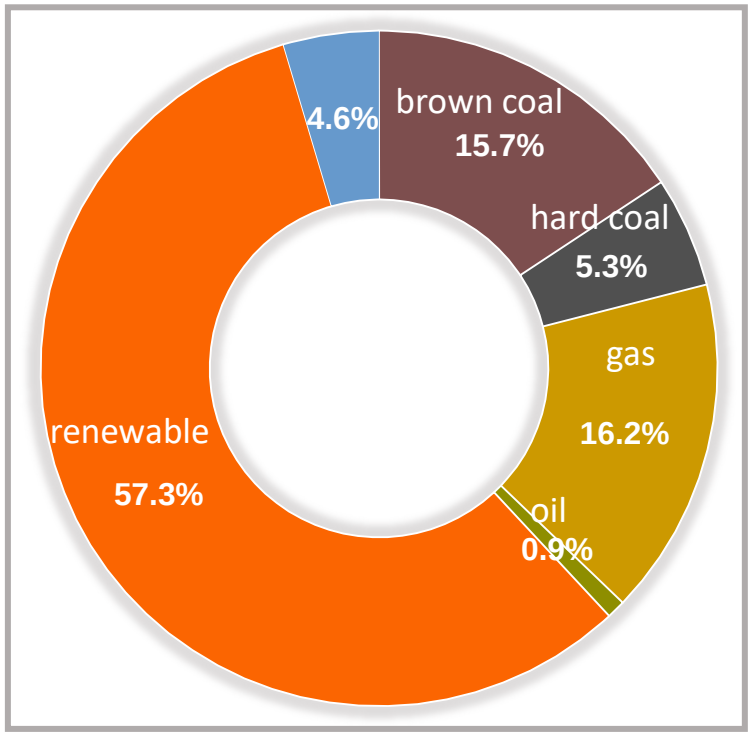

PV in 2024 … 74.1 TWh
… 26.1% of renewables

Source: Statistisches Bundesamt

Solar energy conversion (PV) – solar cell

max. theoretical power conversion efficiency (PCE)
~ 30 % (Shockley-Queisser limit*)

solar cell → electricity

Situation in PV in NRW

- 2025: ~ 960.000 installations with >13 GW installed power
- including >1300 solar parks
- 3rd place in the ranking of the federal states (according to MW)

(https://www.lee-nrw.de/themen/solarenergie/)

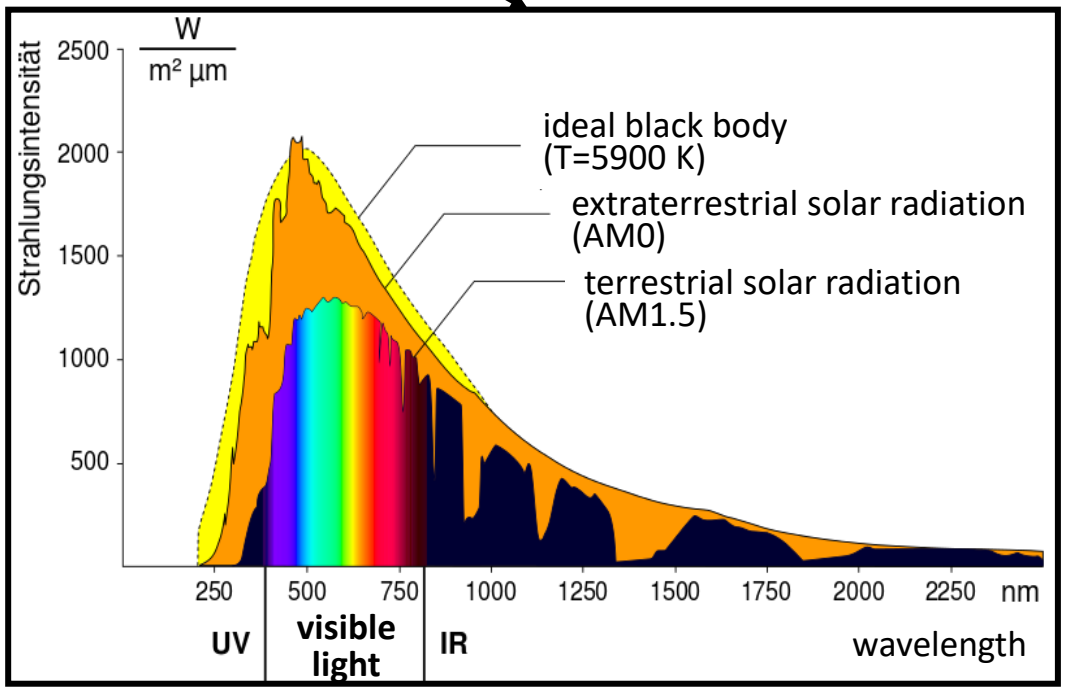

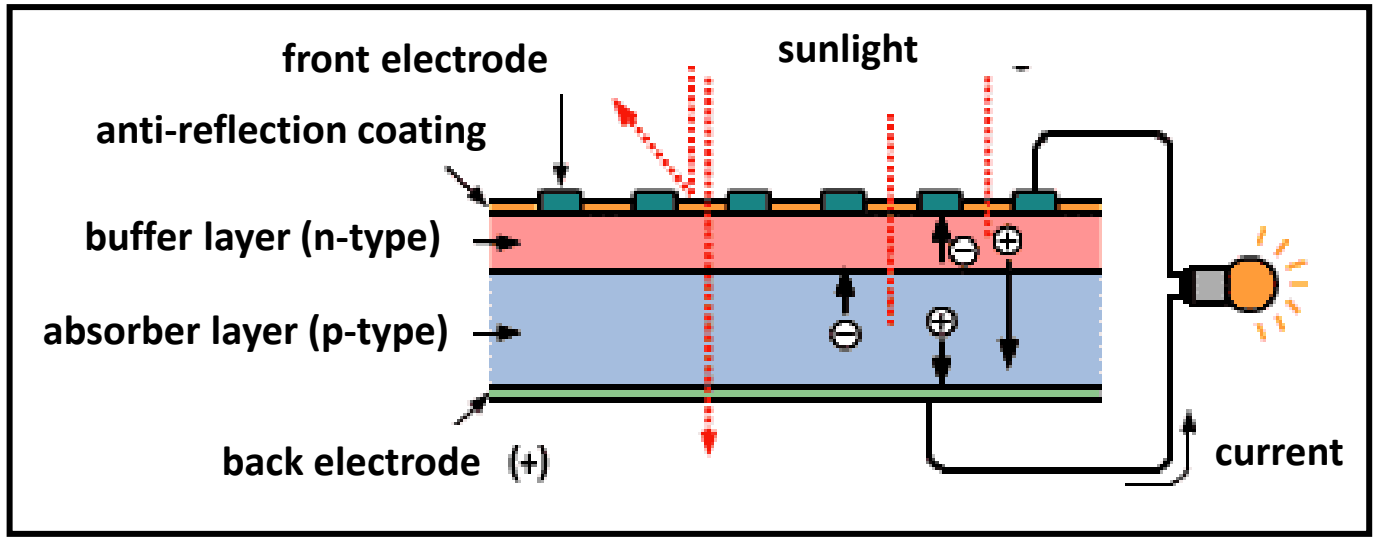

*Shockley & Queisser, J. Appl. Phys. 32 (1961) 510

Absorber materials in thin film solar cells

HZB Helmholtz Zentrum Berlin

CHALCOPYRITES

2nd generation solar cells

thin film solar cell technology with the **highest efficiency**

$Cu(In,Ga)Se_2$ … CIGS

PCE = 23.6 %

- 👍 long term stable
- 👎 In is a scarce element
- 👎 further increase of PCE to be competitive with c-Si

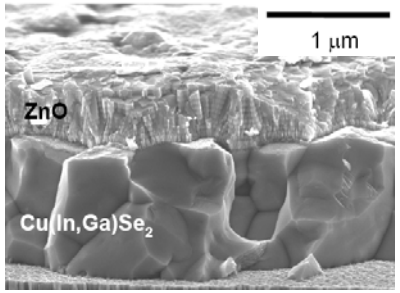

KESTERITES

emerging PV

only **critical raw material** (CRW) free PV technology

$Cu_2ZnSn(S,Se)_4$ … CZTSSe

PCE = 16.6 %

- 👍 long term stable
- 👍 only critical raw material free technology
- 👎 PCE level

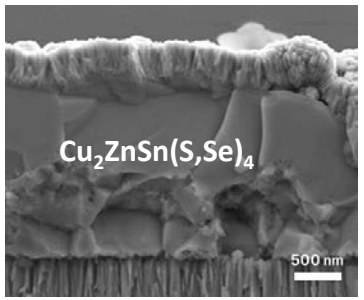

HYBRIDE PEROVSKITES

emerging PV

low cost technology with **high efficiency** devices

$(Cs,MA,FA)\,Pb(I,Br)_3$

PCE = 27.3 %

- 👍 **Perovskite/Si tandem** PCE = 31.3 %
- 👎 lead toxicity
- 👎 material and device instability

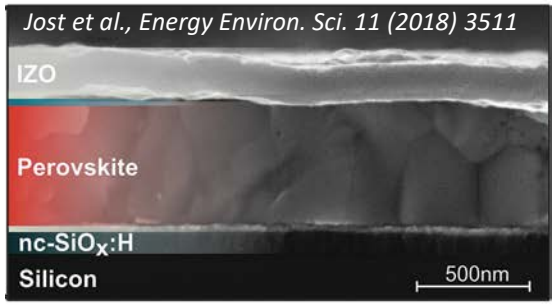

TERNARY NITRIDES

possible new absorber

earth-abundant alternative to III-V compounds

$ZnGeN_2$, $ZnSnN_2$

$PCE_{theoretical}$ = 22 %

- 👍 band gap energy tuning by cation disorder
- 👎 only simulated device efficiency so far

NREL chart best research-cell efficiencies
www.nrel.gov/pv/cell-efficiency.html

PV applications in space

photovoltaic (PV) technologies are at the forefront of enabling space missions and deep space exploration

→ thin film solar cells are promising candidates because of their appealing properties such as lightweightness, flexibility and cost-effective manufacturing

$Cu(In,Ga)(S,Se)_2$	- Geostationary transfer orbit for 1.1 years in 2002–2003/ Sun-synchronous orbit for ~1.6 years in 2005–2006 - low-earth orbit (LEO) for ~1 years in 2009
$Cu_2ZnSn(S,Se)_4$	ISS for 6 months in 2016 and 2019 (Si/CZTS tandem)
CdTe	LEO for 3 years in 2017–2019
hybrid halide perovskites	sub-orbital rocket flight (70–239 km altitude) for 6 min in 2019 ISS for 10 months in 2020

Wing Yi Ho-Baillie, Nature Review Materials 9 (2024) 759

- longer missions (several years) → PV devices in conjunction with rechargeable batteries are the only available option to provide uninterrupted, sustainable and stable electrical power

PV applications in space → harsh conditions → radiation and <u>low temperatures</u>

- lowest temperature on Moon (dark side) → 25 K
- temperature in outer space → can go down to 3 K
- extreme temperature swings occur

Low temperature behaviour of absorber materials in solar cells potentially used in space applications?

Structure – property relationships

atomic structure

3-dimensional periodic arrangement of atoms/ions/…
local / average

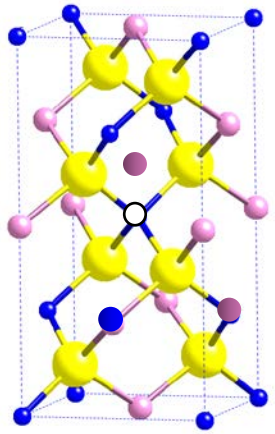

structural disorder

… in the real world → point defects

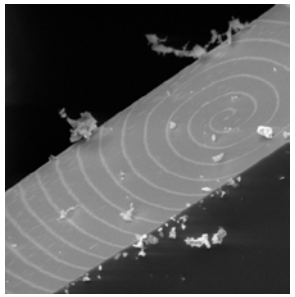

dislocation in $CuGaS_2$

microstructure

- 0D … point defects
- 1D … dislocations
- 2D … stacking faults, grain boundaries
- 3D … inclusions

direct and sunlight-matched optical band gap

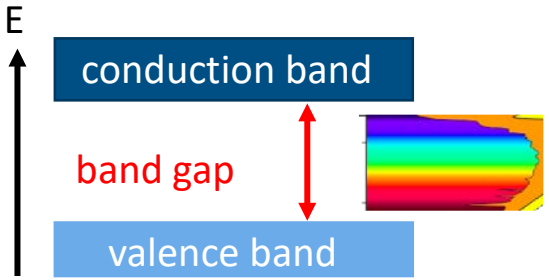

defect tolerance

tendency of a semiconductor to keep its properties despite the presence of crystallographic defects

strong optical absorption

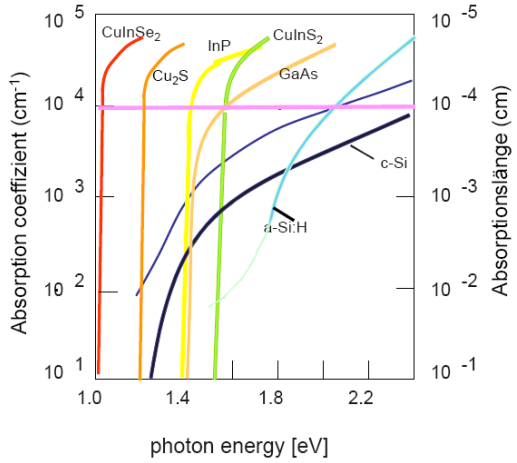

structure — **property** — **function** relationship → **application**

absorption of solar light (photons)

thin film solar cell with increased efficiency

know

engineer

tailor-made materials

optimized application

Why neutrons?

advantages

- wavelength can be easily varied to match atomic spacings
- neutrons have zero charge → not strongly attenuated by furnaces etc.
- neutrons interact with the nucleus of constituent atoms → nuclear interaction

→ can „see“ low-Z elements easily (like H)
→ elements with similar atomic number can have very different contrast

- low energies → non-destructive probe
- energies in the range of collective motions → can study e. g. phonons
- neutrons have a magnetic dipole moment → can study magnetic structures

disadvantages

- neutrons are expensive to produce → access not easy
- neutrons interact weakly with matter → often require large samples
- available fluxes are low compared to those for X-rays

Bertram Brockhouse, Nobel Laureate in Physics 1994

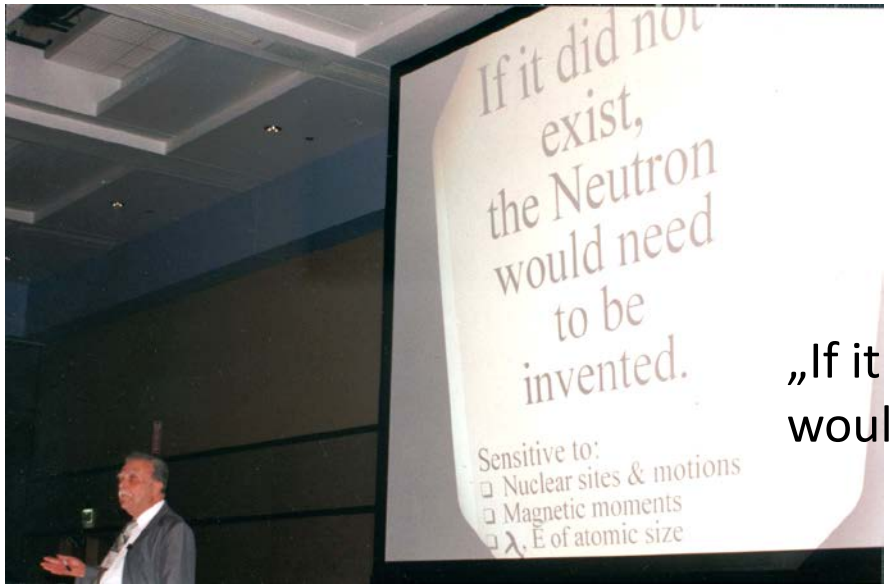

B. Brockhouse at the IUCr Congress 1996 in Seattle, US

„If it did not exist, the Neutron would need to be invented.“

Large scale facilities: neutron sources worldwide

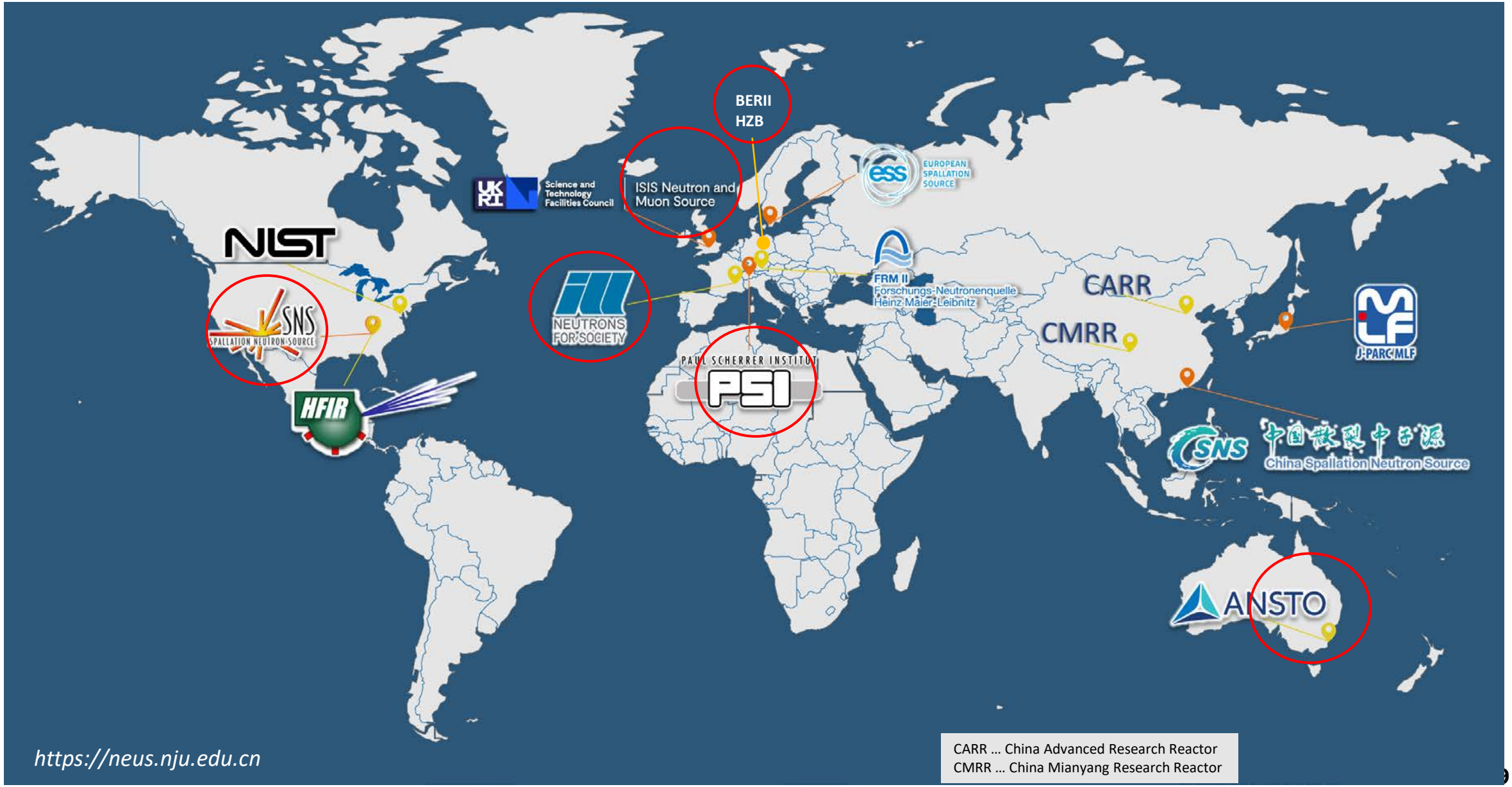

https://neus.nju.edu.cn

CARR … China Advanced Research Reactor
CMRR … China Mianyang Research Reactor

Large scale facilities: synchrotron radiation sources worldwide

Source: ESRF

What we are doing on large scale facilities …

NEUTRONS

neutron diffraction

chalcogenides

- crystal structure
- structural disorder
- crystal structure at low temperatures (T_{min}=1.5K)

hybrid halide perovskites

- crystal structure
- orientational disorder of the molecules

ternary nitrides

- crystal structure & disorder

quasielastic neutron scattering QENS

hybrid halide perovskites

- dynamic structure
- rotations of the molecule

SYNCHROTRON X-RAYS

X-ray diffraction

chalcogenides

- order-disorder transition
- crystal structure at high temperatures (T_{max}=1000 °C)

hybrid halide perovskites

- crystal structure at low temperatures (T_{min}=25K)

small angle X-ray scattering SAXS

hybrid halide perovskites

- early stage of crystallization (agglomerates in precursor solutions)

structural disorder – off-stoichiometry – band gap energy

in quaternary chalcogenides

Kesterites – solar absorber in the only CRM-free thin film PV technology

HZB Helmholtz Zentrum Berlin

→ compound semiconductors **crystallizing in the Kesterite-type structure**

→ general chemical formula $A^{I}_{2}B^{II}C^{IV}X^{VI}_{4}$

→ constituent elements are abundant and eco-friendly

Cu_2ZnSnS_4 (CZTS)
$Cu_2ZnSnSe_4$ (CZTSe)
$Cu_2ZnSn(S,Se)_4$ (CZTSSe)

→ **solar cell efficiency**

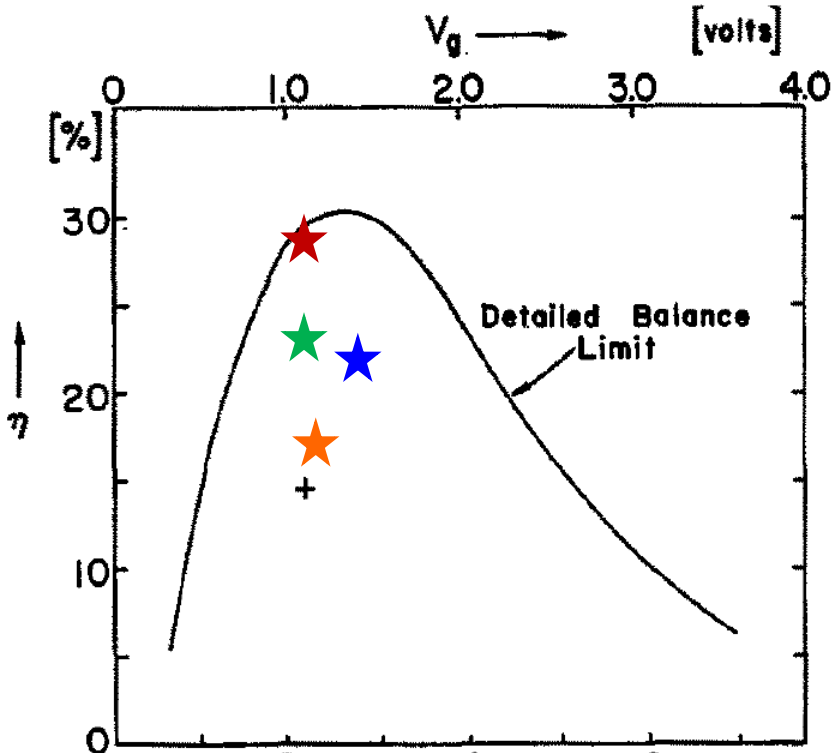

Shockley-Queisser limit (detailed balance limit)

Shockley&Queisser, J. Appl. Phys. 32 (1961) 510

absorber	efficiency 2026	year of first reported efficiency
Si	27.9%	1954 (Bell Labs)
$Cu(In,Ga)Se_2$	23.6%	1977 (Uni Maine, $CuInSe_2$)
CdTe	22.4%	1970er/80er
$Cu_2ZnSn(S,Se)_4$	16.6%	1996 (Nagaoka NCT)

certified efficiencies in:
Best Research-Cell Efficiency Chart, NREL, www.nrel.gov/pv/cell-efficiency.html

Chalcopyrite- vs. Kesterite-based thin film solar cells

Kesterite is currently the **most promising emerging fully inorganic thin film photovoltaic technology** based on **critical raw-material-free materials** (CRM) and **sustainable** solutions. [1]

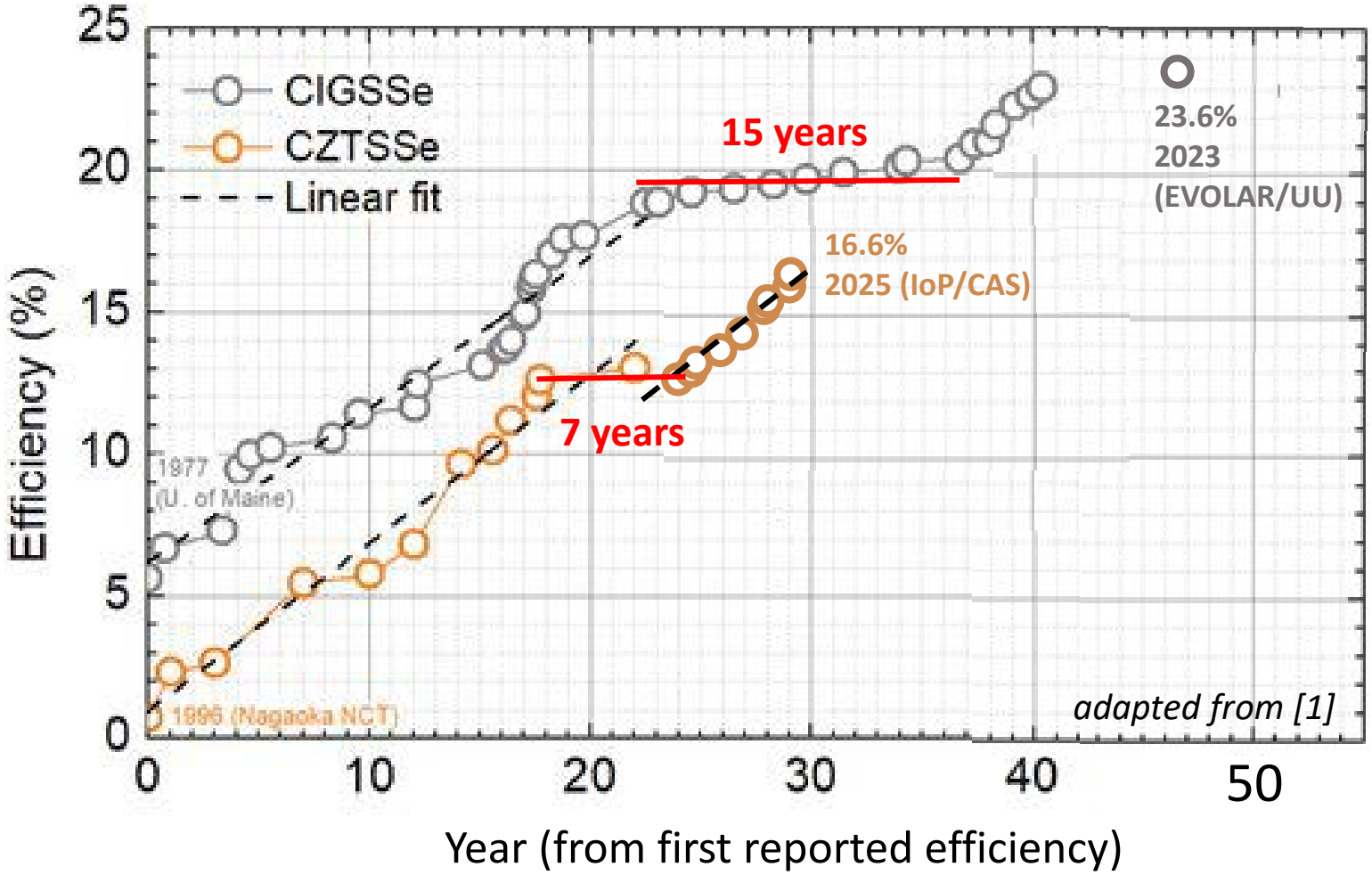

Chalcopyrites

CIGSSe … $Cu(In,Ga)(S,Se)_2$

first reported efficiency: 1977

slope: 0.53

Kesterites

CZTSSe … $Cu_2ZnSn(S,Se)_4$

first reported efficiency: 1996

slope: 0.59

[1] Giraldo et al. Adv. Mater. 31 (2019) 1806692

Defects play a crucial role: intrinsic doped semiconductors

HZB Helmholtz Zentrum Berlin

	$Cu(In,Ga)Se_2$	$Cu_2ZnSn(S,Se)_4$
	Chalcopyrites	**Kesterites**
	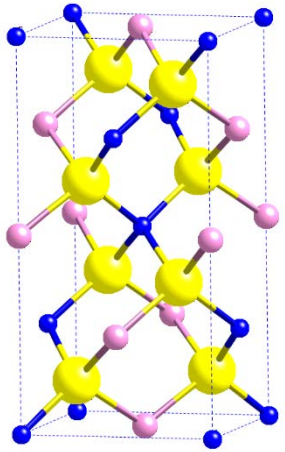	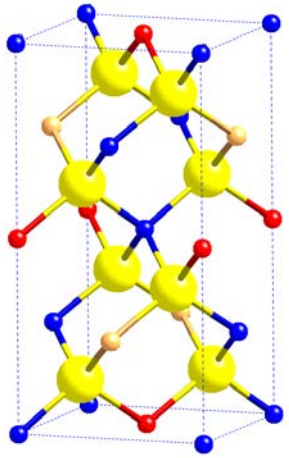
	Chalcopyrite type crystal structure	**Kesterite type crystal structure**

→ intrinsic semiconductors

→ intrinsically doped by point defects

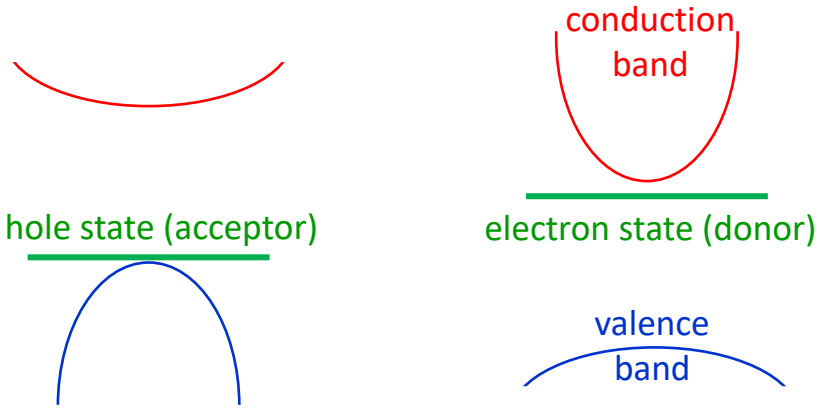

copper vacancies (V_{Cu}) → dominant intrinsic defect

→ causes p-type conductivity

→ shallow acceptor

complex point defect scenario

- alteration of optoelectronic properties p – type/n – type conductivity
- defects introduce energy levels (traps) in the band gap → annihilate charge carriers (Shockley-Read-Hall recombination-SRH)
- deep defects act as recombination centers

shallow defects → low SRH rates → beningn → „good“ defect

deep defects → high SRH rates → detrimental → „bad“ defect

Flexibility of the crystal structure and off-stoichiometry

Kesterite-type structure is very flexible and can stabilize point defects (vacancies, anti sites, interstitials)

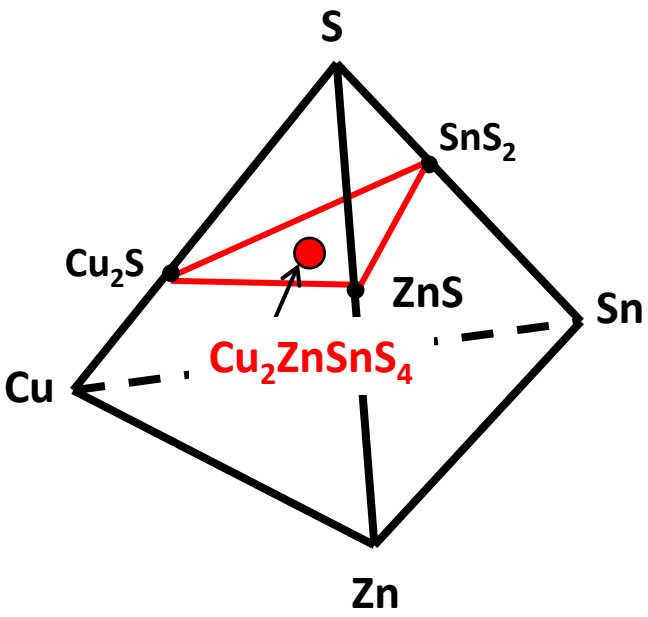

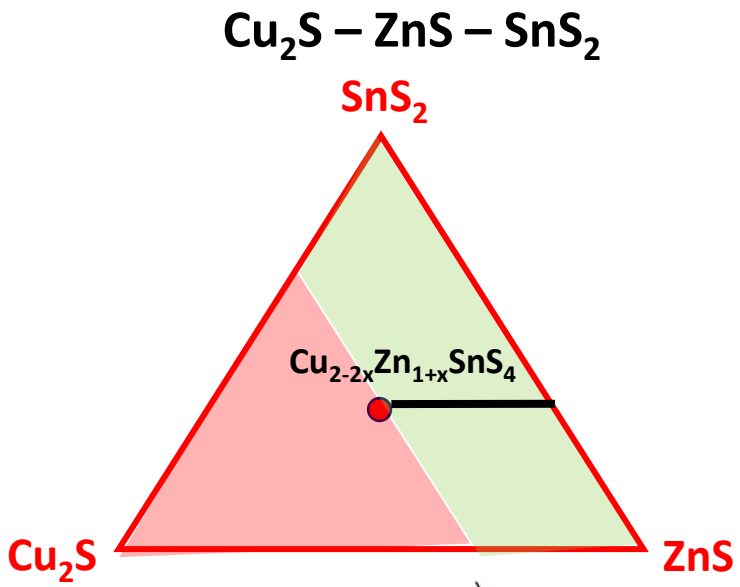

off-stoichiometry relations

Cu/(Zn + Sn) < 1	Zn/Sn > 1
Cu/(Zn + Sn) < 1	Zn/Sn < 1
Cu/(Zn + Sn) > 1	Zn/Sn > 1
Cu/(Zn + Sn) > 1	Zn/Sn < 1

cation ratio plot

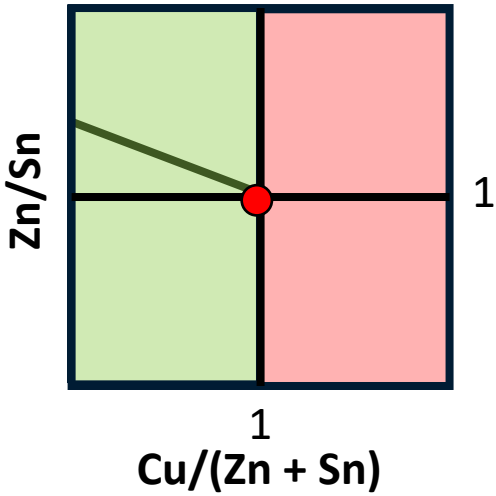

off-stoichiometry type model (A- … L-ype)
correlates off-stoichiometric composition and intrinsic point defects
Example: A-type … V_{Cu} & Zn_{Cu}

→ defines existence regions for each point defect type

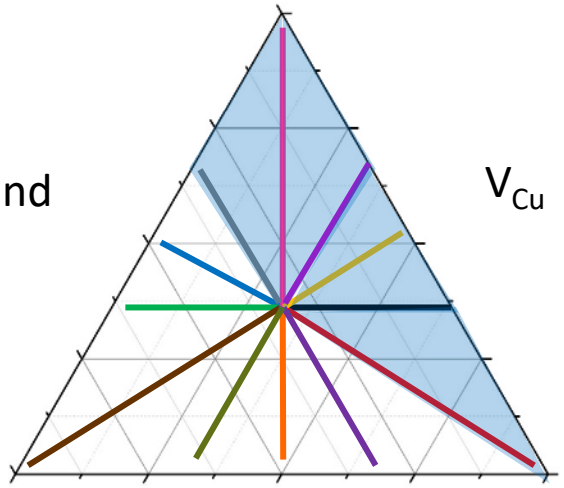

- **Kesterite-type structure can adapt strong deviations from stoichiometry without a collapse of the crystal structure**
- **12 intrinsic point defects**
  3 cations (Cu^{+}, Zn^{2+}, Sn^{4+}) →
  (3 vacancies + 3 interstitials + 6 anti-sites)

A-D type: *A. Lafond et al., Z. Anorg. Allg. Chem. 638 (2012) 2571* G-L-type: *G. Gurieva, Schorr et al., Journal of Applied Physics 123 (2018) 161519*

Intrinsic point defects in kesterites

Intrinsic defects introduce energy levels (traps) in the band gap

CZTS

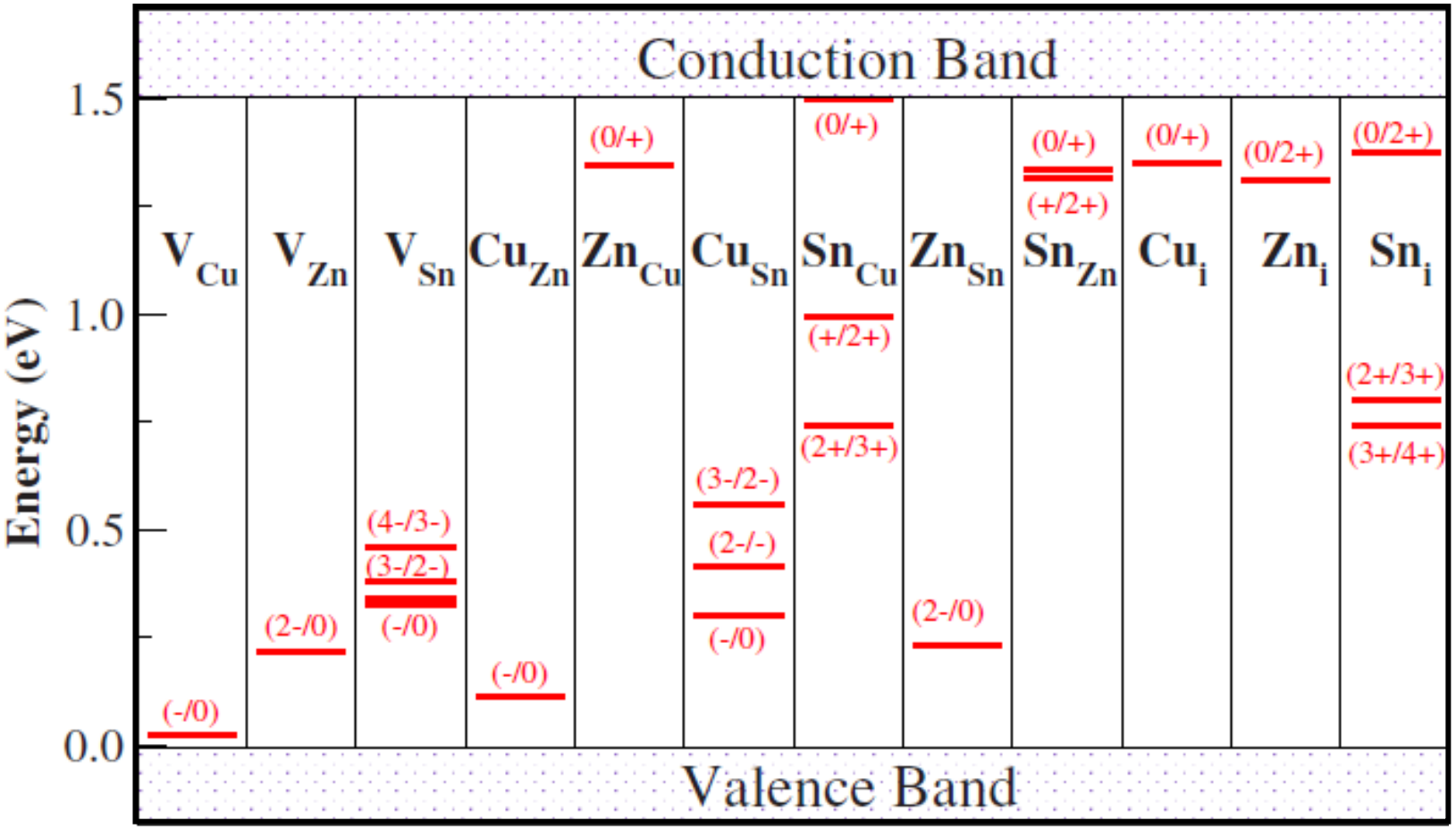

midgap defects: Zn_{Cu} Zn_{Sn} Sn_{Zn} V_{Sn} Zn_i

deep defect: Cu_{Sn} Sn_{Cu}

not favourable: Cu_i

→ annihilate charge carriers (Shockley-Read-Hall recombination-SRH)

shallow defects: V_{Cu} Cu_{Zn} Zn_{Cu}

intrinsic point defects in high concentrations (10^{19} – 10^{20} defects/cm³)

→ structural disorder

S. Chen et al, Phys Rev 81 (2010) 245204

T. Maeda et al., Jpn. J. Appl. Phys. 50 (2011) 04DP07

Structural perception of intrinsic point defects

HZB Helmholtz Zentrum Berlin

defect levels obtained by spectroscopy (e. g. PL)

BUT: very little evidence exists as to the **chemical and structural identification of the defect** producing those levels

crystal structure analysis by X-ray diffraction **and neutron diffraction**

⇒ **point defects change significantly the scattering cross section σ_{coh} of the cation structural sites**

scattering cross section σ_{scat} is a hypothetical area which describes the likelihood of X-rays / neutrons being scattered by an atom / nucleous

$Cu(In,Ga)S_2$ $Cu(In,Ga)Se_2$

Cu_2ZnSnS_4 $Cu_2ZnSnSe_4$

Cu_2ZnGeS_4 $Cu_2ZnGeSe_4$

$ZnGeN_2$

X-ray diffraction

$\sigma_{coh} \sim f^2$

BUT: Cu, Zn, Ga and Ge are electronic similar elements

Cu^+, Zn^{2+}, Ga^{3+} and Ge^{4+} are isoelectronic

→ equal atomic scattering factor f

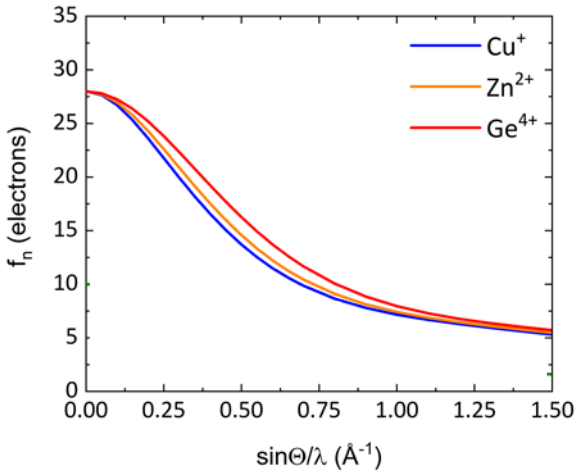

→ different neutron scattering length b

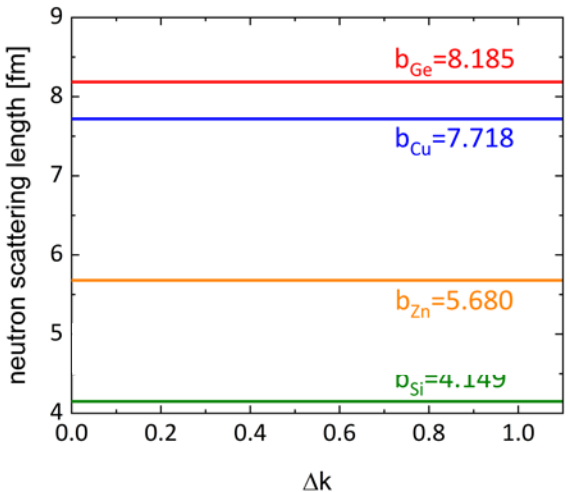

neutron diffraction

$\sigma_{coh} \sim b^2$

Experimental determination of intrinsic point defects (type & concentr.)

Average neutron scattering length analysis method

Schorr et al. in: Advanced characterization techniques for thin film solar cells, Wiley, 2016

pre-requesit → determination of **chemical composition** of quaternary phase by **WDX** spectroscopy
→ homogeneous powder sample

neutron diffraction

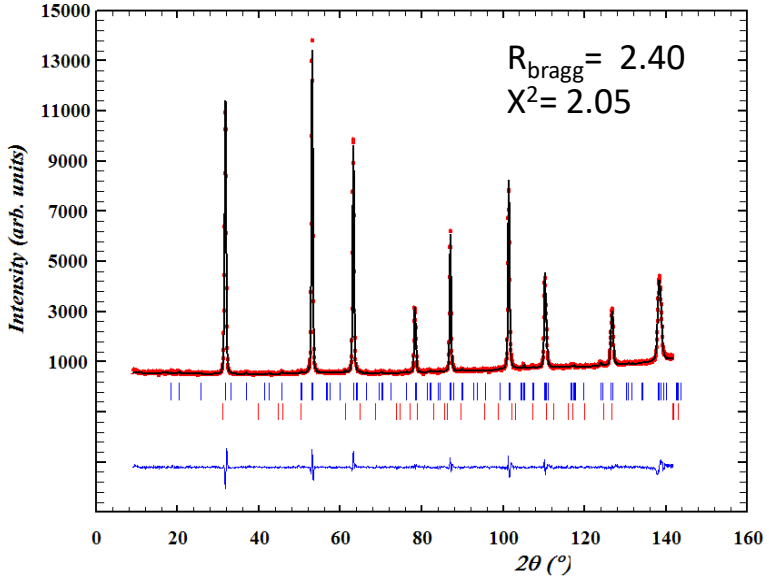

average neutron scattering lengths

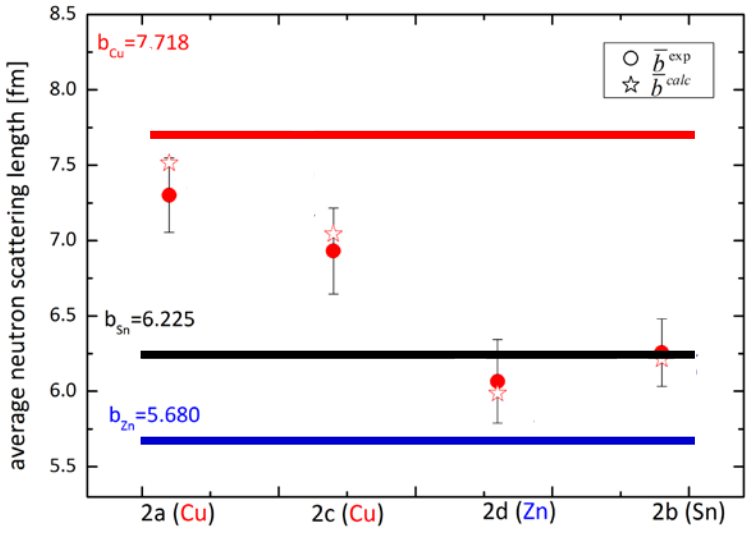

cation distribution model

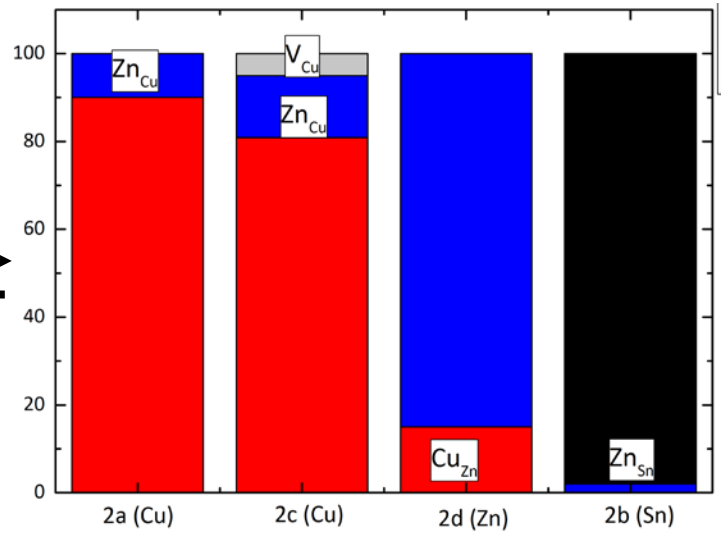

simultaneous Rietveld analysis of diffraction data (X-ray & neutron)

site occupancy factors (SOF)

$$\bar{b}_j(\text{exp}) = SOFj \cdot b_k$$

j … Wyckoff site, k … cation

average neutron scattering length analysis

minimizing the difference between $\bar{b}^{exp}$ and $\bar{b}^{calc}$ by varying the cation distribution

$$\bar{b}_j(calc) = \sum_k (k)_j^{model} \cdot b_k$$

intrinsic point defects

- type (qualitative!)
- concentration (quantitative!)

Cu-Zn disorder in kesterite-type materials (kesterites)

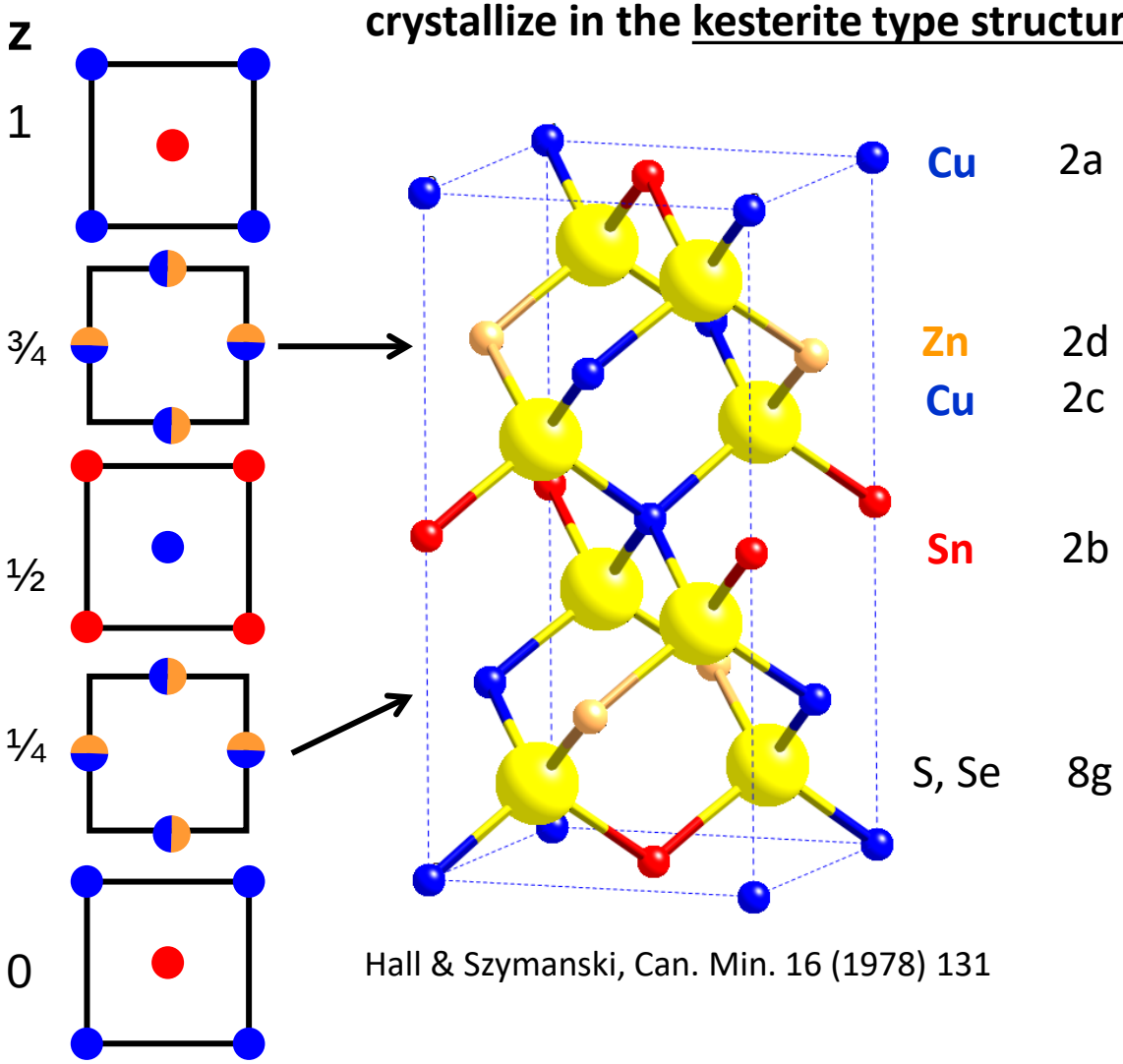

Hall & Szymanski, Can. Min. 16 (1978) 131

Cu_2ZnSnS_4, $Cu_2ZnSnSe_4$ and $Cu_2ZnGeSe_4$ crystallize in the kesterite type structure

with Cu/Zn disorder occurs in the planes with z=¼ and ¾

discovered in 2005 in Cu_2ZnSnS_4 by neutron diffraction, published in 2007

Cu_{Zn} and Zn_{Cu}

defect concentration 10^{20} to 10^{21} cm^{-3}

Cu/Zn disorder

→ **disordered kesterite**

order parameter Q

$$Q = \frac{[Cu_{2c} + Zn_{2d}] - [Zn_{2c} + Cu_{2d}]}{[Cu_{2c} + Zn_{2d}] + [Zn_{2c} + Cu_{2d}]}$$

Q=1 → order (Cu – 2c, Zn – 2d)
Q=0 → complete disorder

Schorr et al., Europ. J. Mineral. 19 (2007)

Schorr et al., Sol En Mat Sol Cells 95 (2011) 1482

Valakh, Schorr et al., Phys. Status Solidi (RRL) 7 (2013) 258

Többens, Schorr et al., Phys Stat Sol B 253 (2016) 1890

The Cu/Zn order – disorder phase transition

Lattice parameter obtained by ***in-situ*** **synchrotron X-ray diffraction (ESRF)**

→ first hint for a change in cation distribution

CZTS

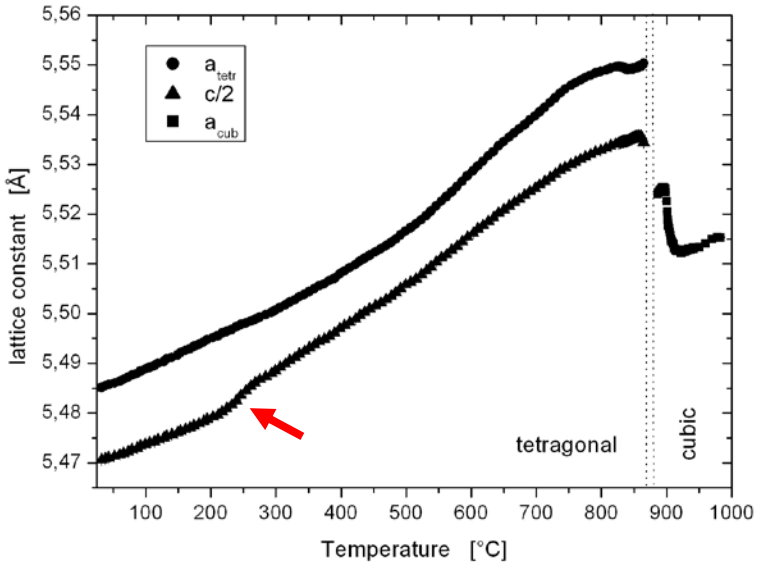

T_C (CZTS) ≅ 240 – 260 °C

order-disorder transition described qualitatively by
the **ratio of two Raman peaks**

$$Q = I(m_{2A})/I(m_{3A})$$

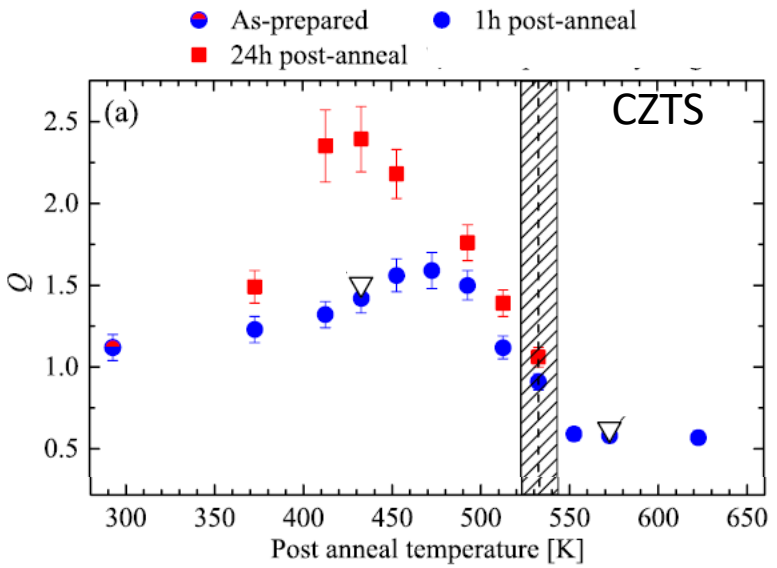

T_C(CTZS) ≅ 260°C

order-disorder transition described quantitatively by
the **site occupancy of 2c and 2d sites** obtained by **MEAD (BESSYII)**

$$Q = \frac{[Cu_{2c} + Zn_{2d}] - [Zn_{2c} + Cu_{2d}]}{[Cu_{2c} + Zn_{2d}] + [Zn_{2c} + Cu_{2d}]}$$

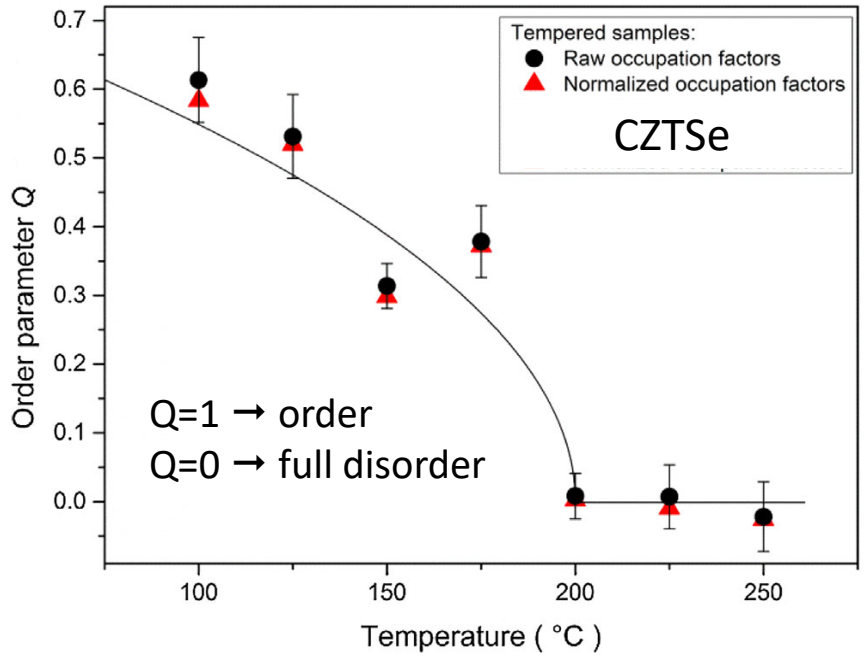

T_C(CTZSe) ≅ 190°C

S. Schorr et al., Phys Stat Sol A 206 (2009) 1054

J. Scragg et al., APL 104 (2014) 041911

Többens, Schorr et al., Phys Stat Sol B 253 (2016) 1890

Correlation of Cu/Zn disorder and optoelectronic properties

HZB Helmholtz Zentrum Berlin

UV-Vis spectroscopy

→ band gap energy E_g increases with decreasing disorder

Q=1 … order

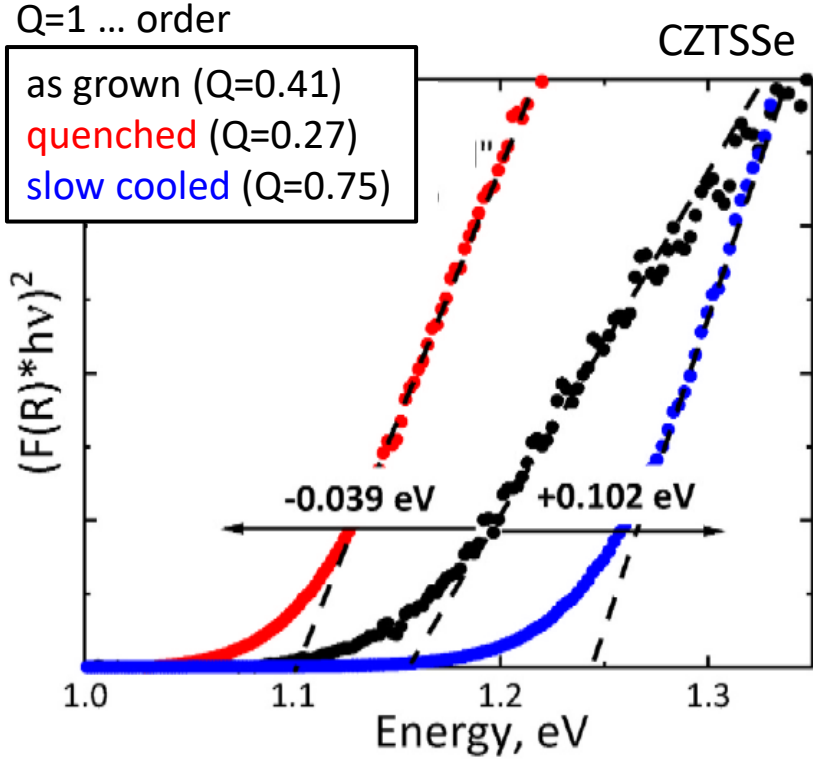

Gurieva, Schorr et al., Sol. En. Mat. Sol. Cells 248 (2022) 112009

Photoluminescence

→ PL_{max} increases with decreasing disorder

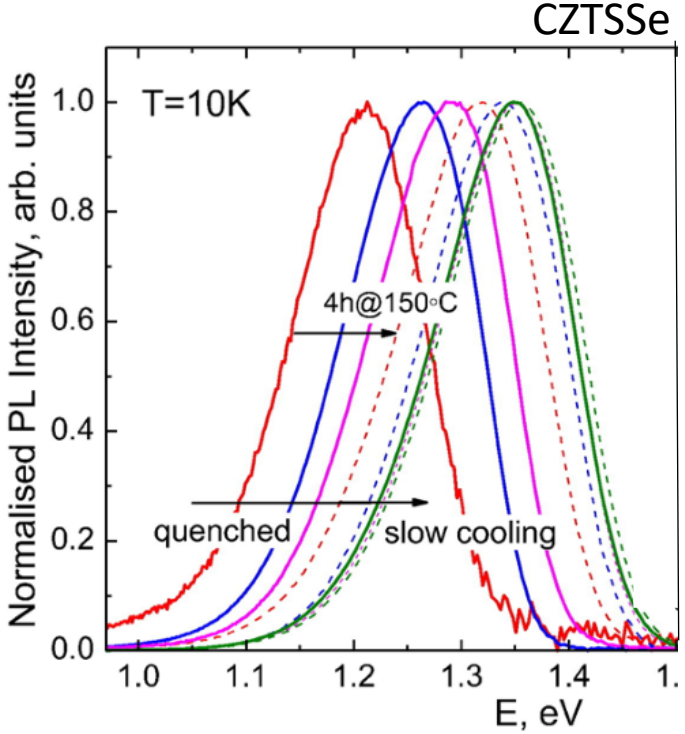

Annealing at $T < T_C$

→ decrease of Cu/Zn disorder

→ increase of V_{OC}

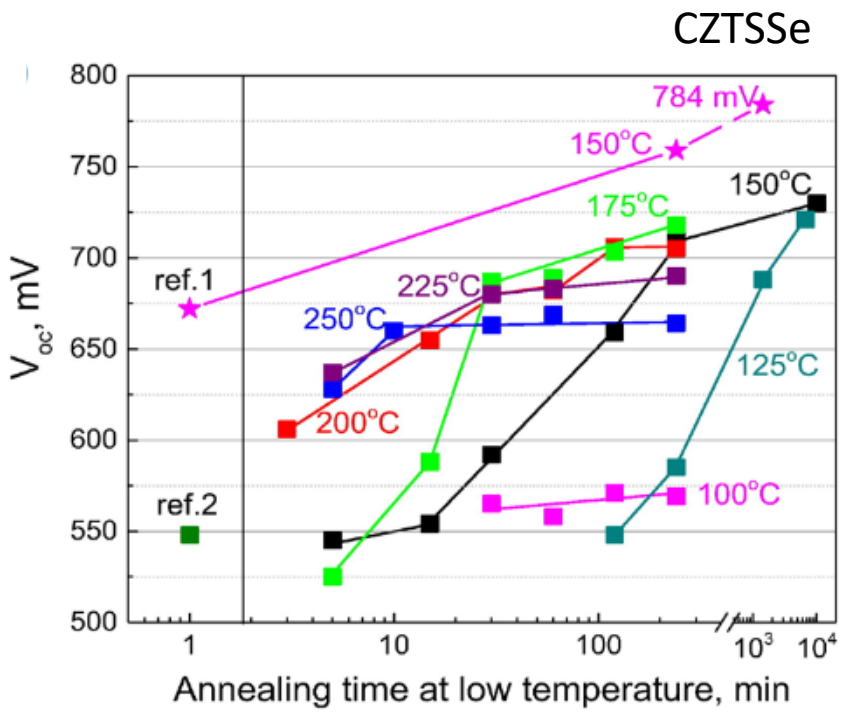

Li et al., npj Flexible Electronics 16 (2023)

Technology development: low temperature annealing ($T < T_C$) as post-deposition treatment of the solar absorber → decrease of Cu/Zn disorder → increase in V_{OC}

Intrinsic point defects in kesterite solar absorbers

HZB Helmholtz Zentrum Berlin

„good" defects

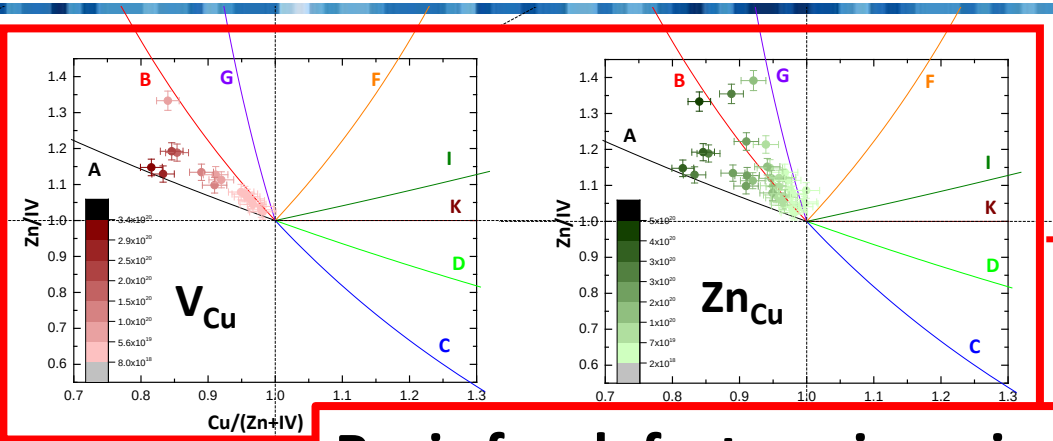

Schorr et al., J. Physics: Energy 2 (2020) 012002

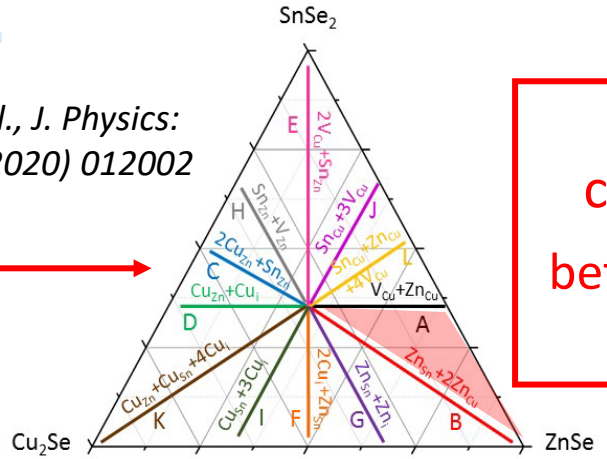

favourable compositional region between A - and B - type V_{Cu} / Zn_{Cu} / Zn_{Sn}

Basis for defect engineering!

„bad" defects

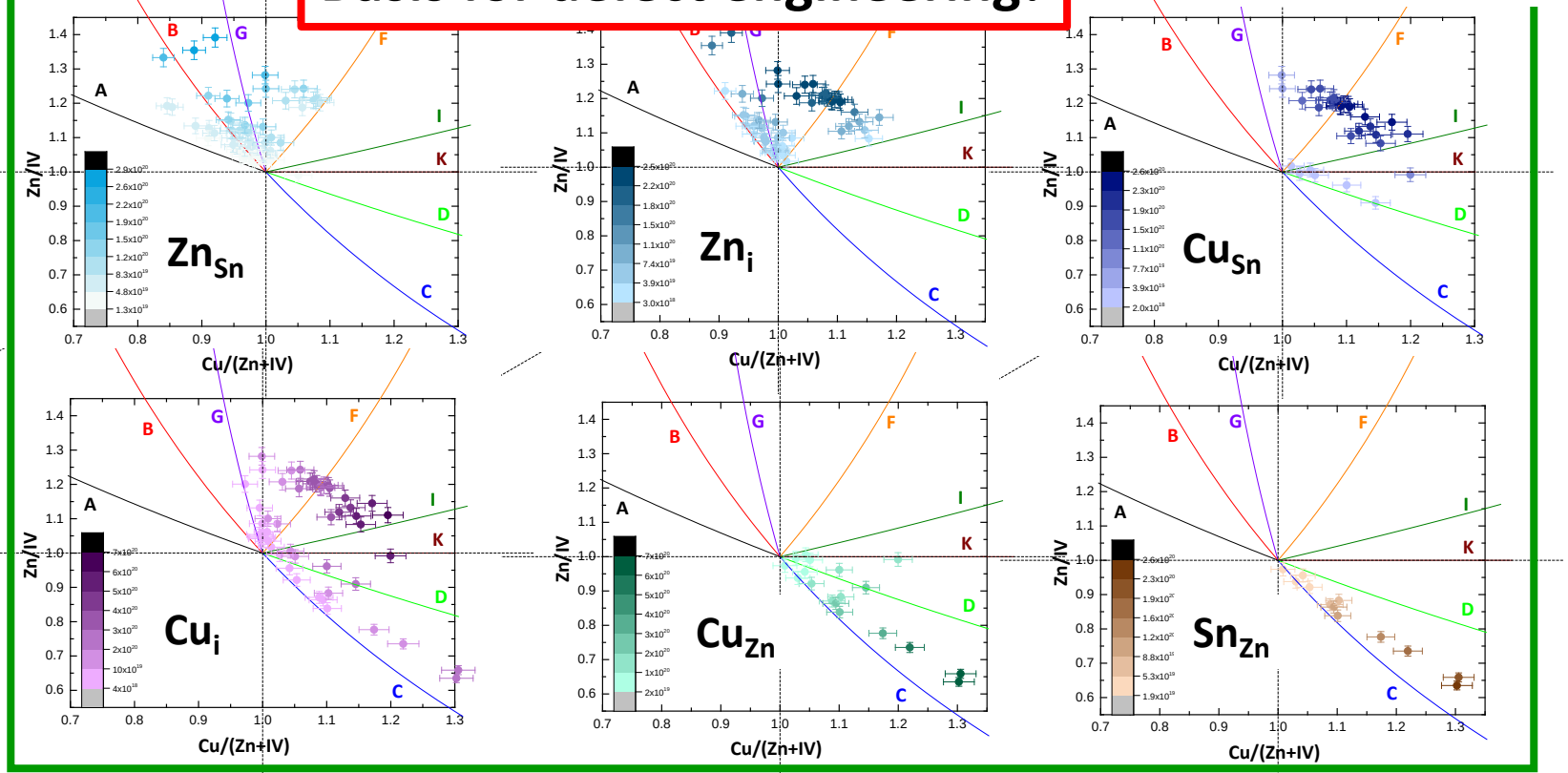

CZTS

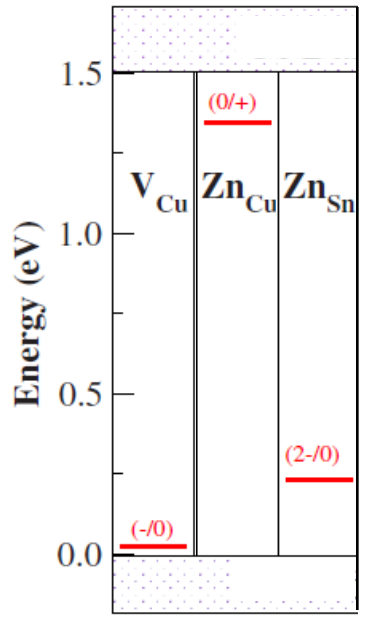

S. Chen et al, Phys. Rev. 81 (2010) 245204

Intrinsic point defects in kesterite-type solar absorbers

HZB Helmholtz Zentrum Berlin

off-stoichiometry type related point defects → 10^{20} – 10^{21} defects/cm^3

cation ratio plot

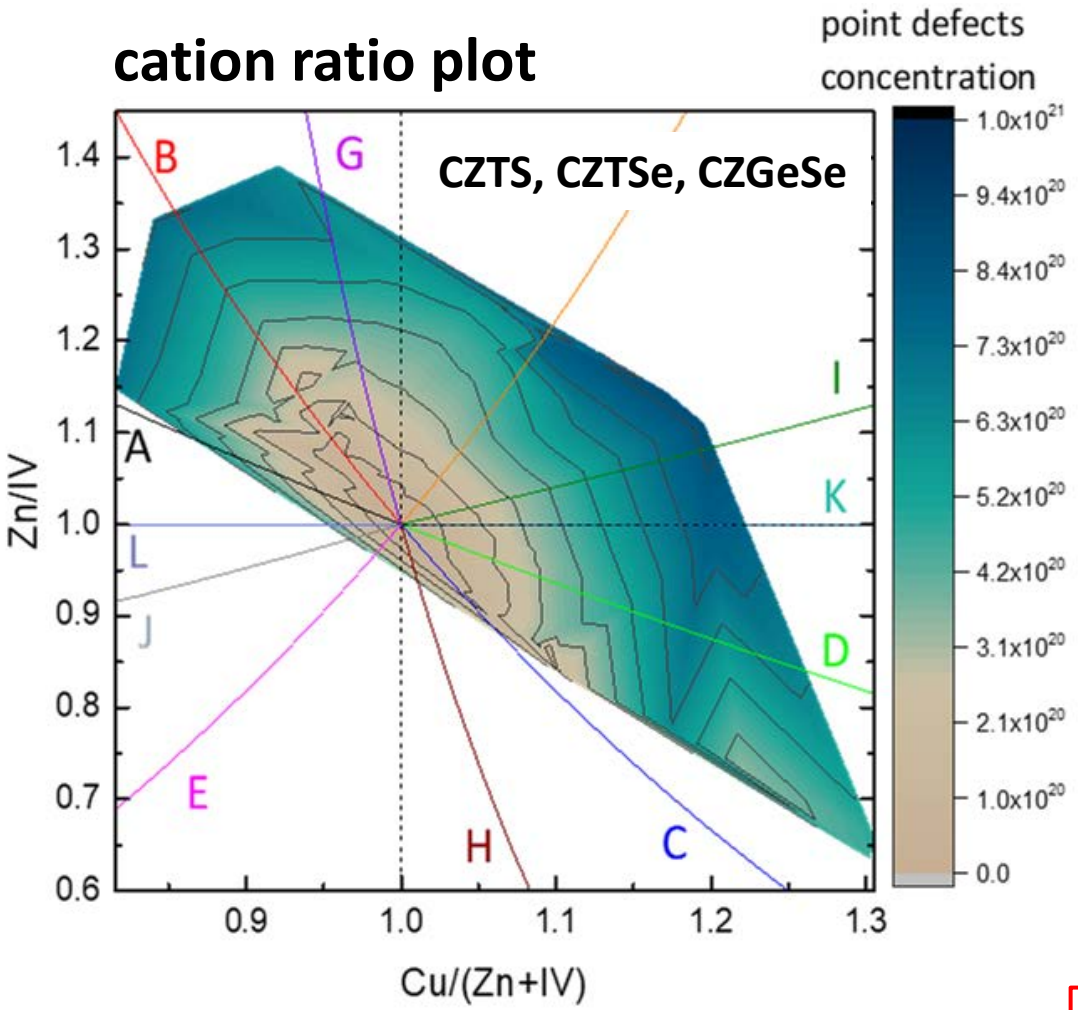

Schorr et al., J. Physics: Energy 2 (2020) 012002
S. Schorr, G. Gurieva in: Crystallography in Materials Research, ed. by S. Schorr and C. Weidenthaler, De Gruyter (2021)

compositional variations of the absorber layer cause

→ variations in type and concentration of point defects

→ band gap fluctuations

→ electrostatic potential fluctuations → decrease V_{OC}

E_g of A-B type CZTSe

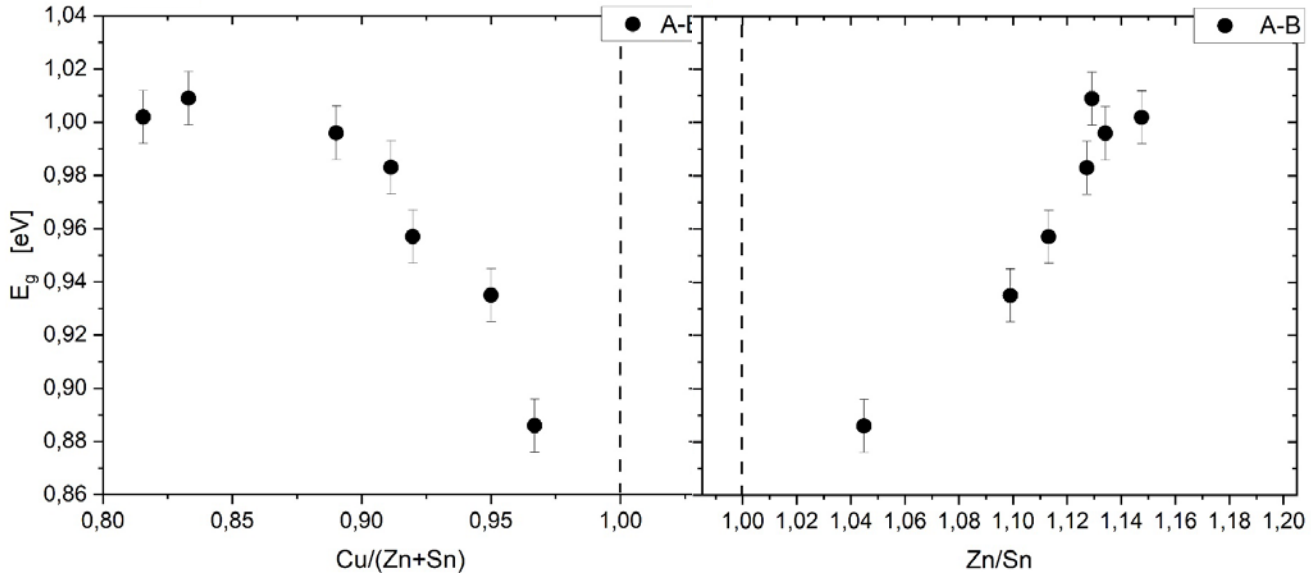

Optimization of the absorber thin film growth process towards chemical homogeneity is crucial!

Take basic research to application: kesterite-based solar cells and beyond

HZB Helmholtz Zentrum Berlin

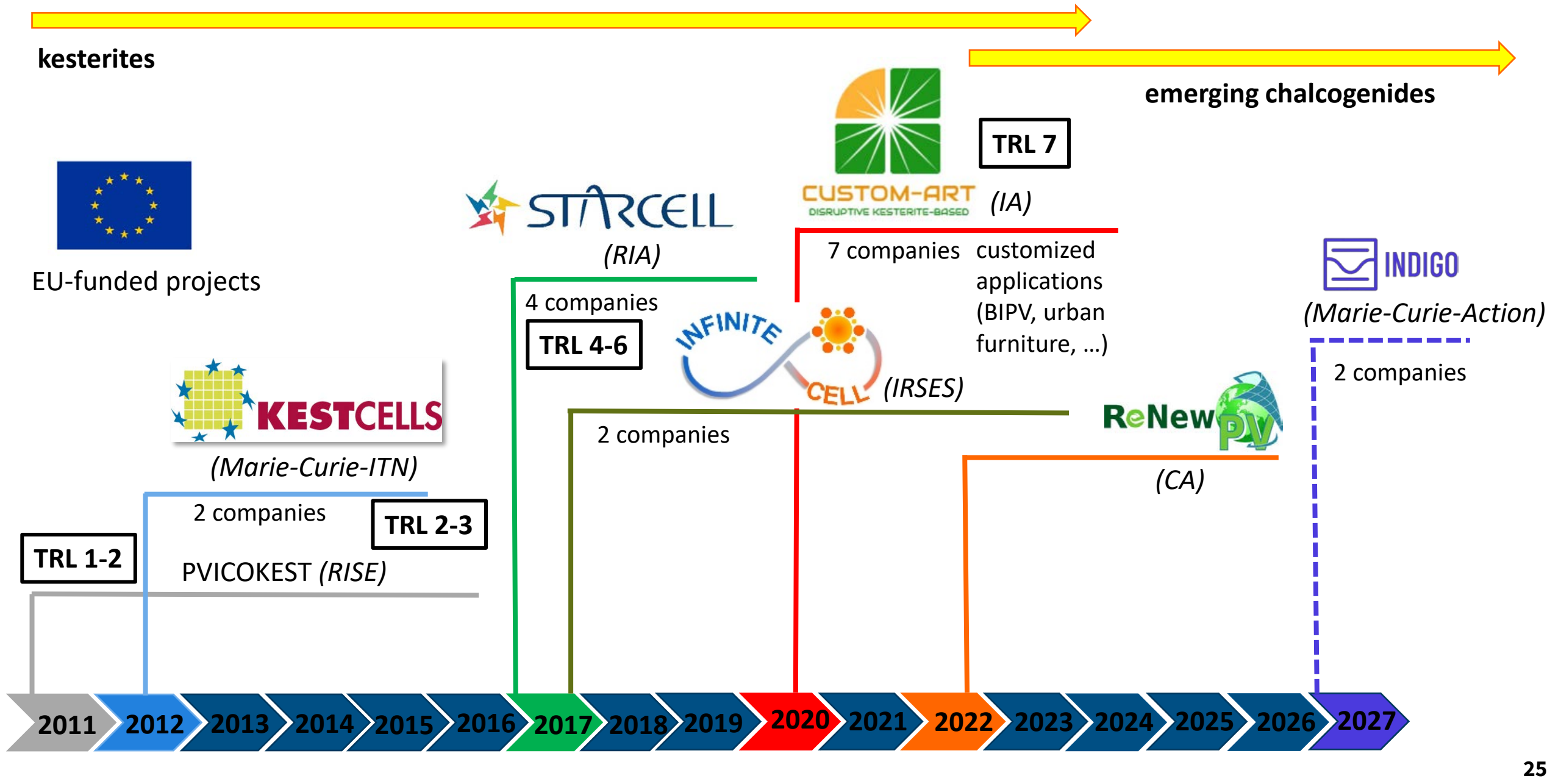

Novel materials for
tandem (and triple junction) thin film solar cell applications

Novel materials for new top and bottom solar cells

HZB Helmholtz Zentrum Berlin

optimal band gap energy as part of a multi-junction stack
Bremner et al., Solar Energy 135 (2016) 750.

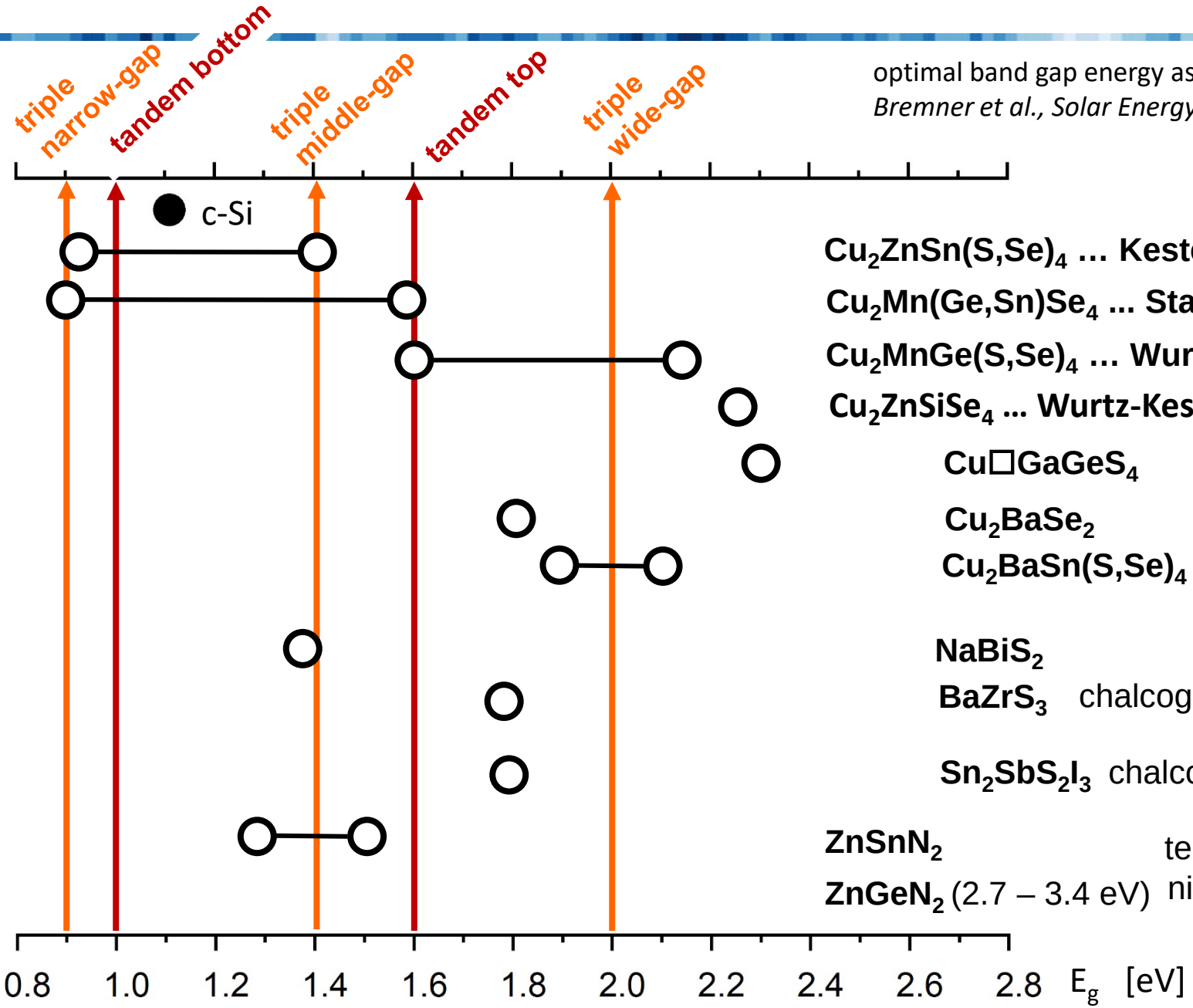

$Cu_2ZnSn(S,Se)_4$ … Kesterite structure

$Cu_2Mn(Ge,Sn)Se_4$ … Stannite/W-Stannite structure

$Cu_2MnGe(S,Se)_4$ … Wurtz-Stannite structure

$Cu_2ZnSiSe_4$ … Wurtz-Kesterite structure

$Cu\square GaGeS_4$

Cu_2BaSe_2

$Cu_2BaSn(S,Se)_4$

$NaBiS_2$

$BaZrS_3$ chalcogenide perovskite

$Sn_2SbS_2I_3$ chalcohalides

$ZnSnN_2$

$ZnGeN_2$ (2.7 – 3.4 eV) ternary nitrides

ReNewPV

COST Action CA21148

renewpv.eu

Research and International Networking on **Emerging Inorganic Chalcogenides** for Photovoltaics

All perovskite triple junction solar cell?

HZB Helmholtz Zentrum Berlin

chalcogenide „kesterites“

→ **possibility to tune the absorption onset a la carte by ion replacement**

→ **lowest possible E_g ~ 0.8 eV**

material is long term stable

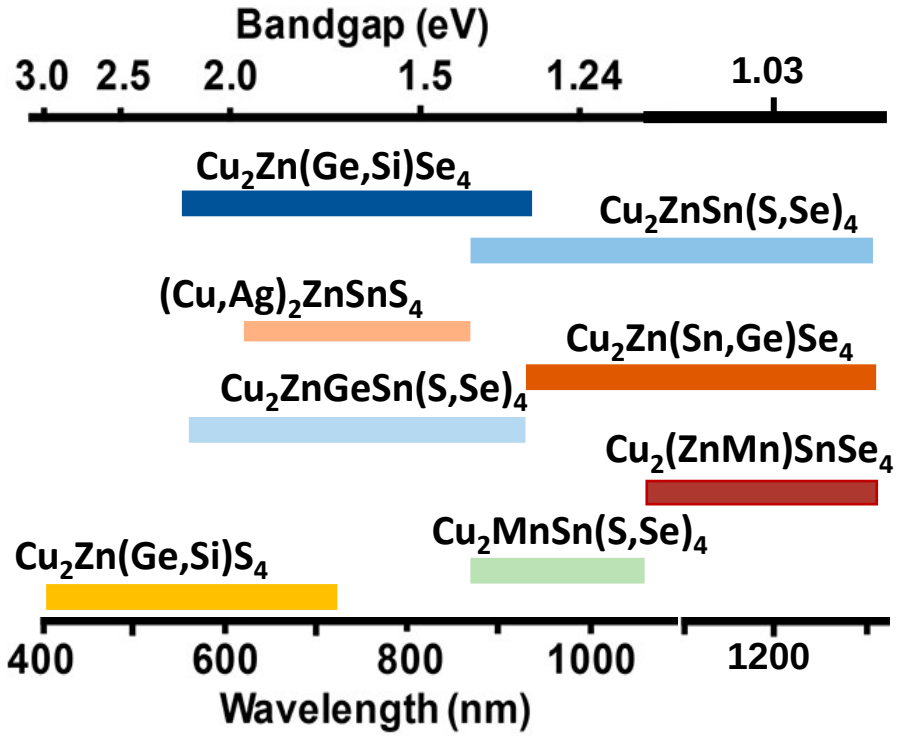

S. Schorr, Sol. En. Mat. Sol. Cells 249 (2023) 112044

halide perovskites

→ **possibility to tune the absorption onset a la carte by ion replacement**

→ **lowest possible E_g ~ 1.2 eV**

material is not long term stable

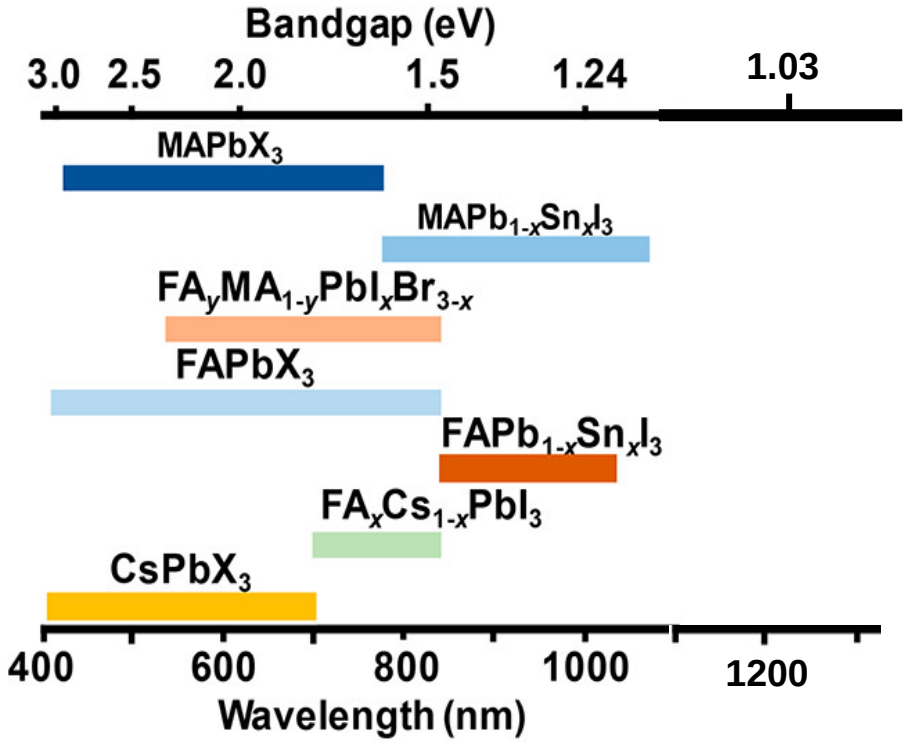

X=I, Br, Cl

M. Anaya et al. Joule 1 (2017) 769-793

Structure relations: sequence of cation layers

HZB Helmholtz Zentrum Berlin

Kesterite

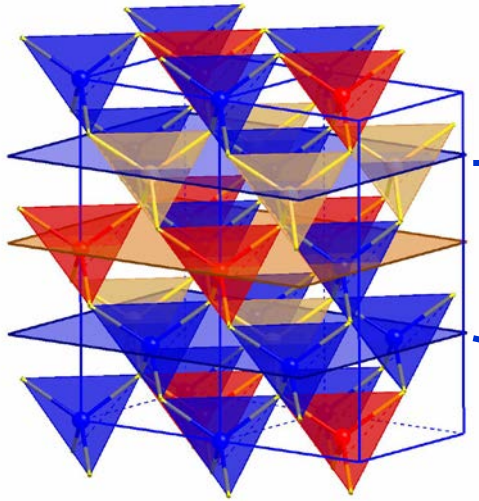

Cu_2ZnSnS_4

cation lattice planes $\perp \vec{c}$

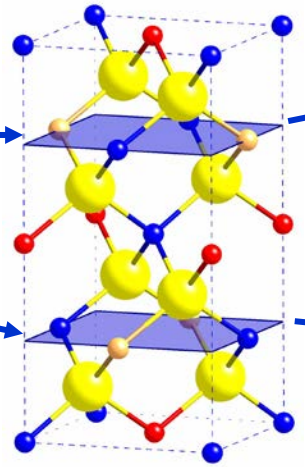

Cu-Zn planes

Cu-Zn planes

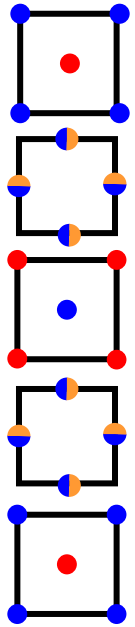

cation lattice planes $\perp \vec{a}$

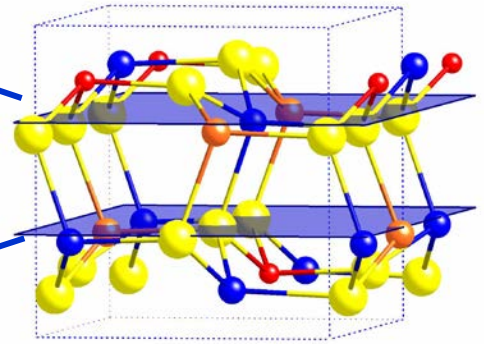

Wurtz-Kesterite

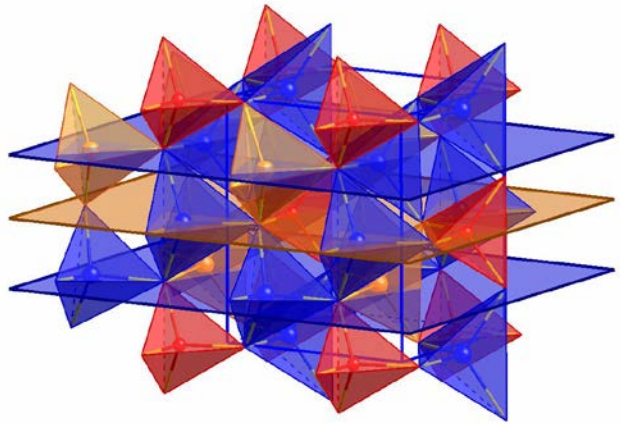

$Cu_2ZnSiSe_4$

Stannite

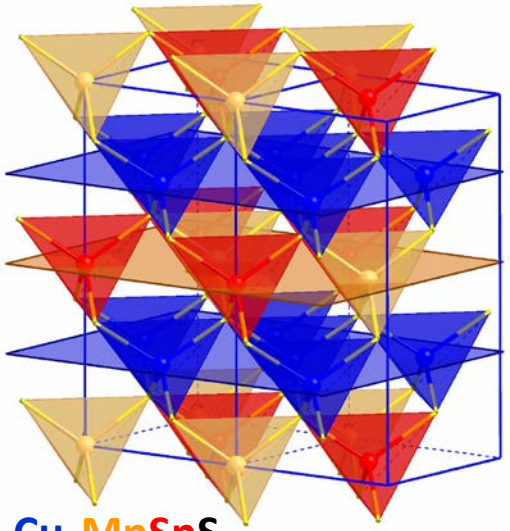

Cu_2MnSnS_4

cation lattice planes $\perp \vec{c}$

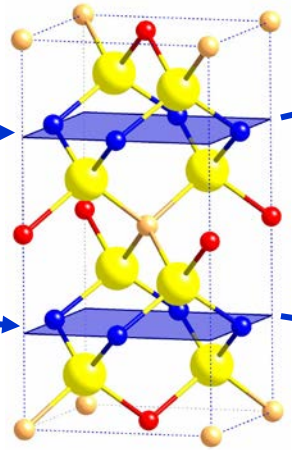

Cu-Cu planes

Cu-Cu planes

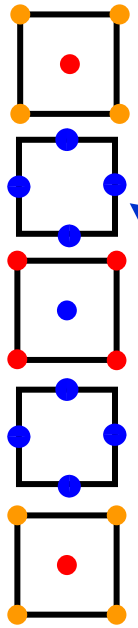

cation lattice planes $\perp \vec{a}$

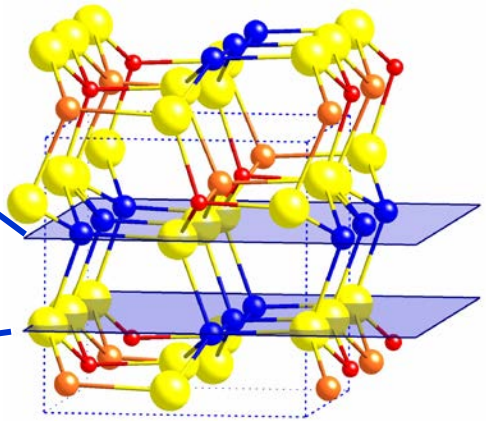

Wurtz-Stannite

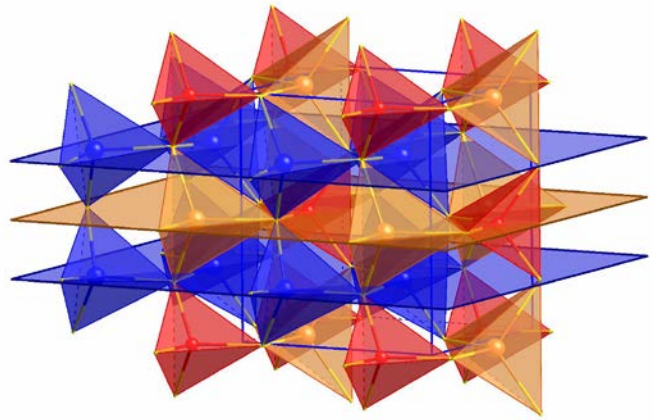

$Cu_2MnSnSe_4$

Neutron powder diffraction & Rietveld refinement (selection)

HZB Helmholtz Zentrum Berlin

G. Gurieva et al., J. Alloys Comp. 846 (2020) 156304

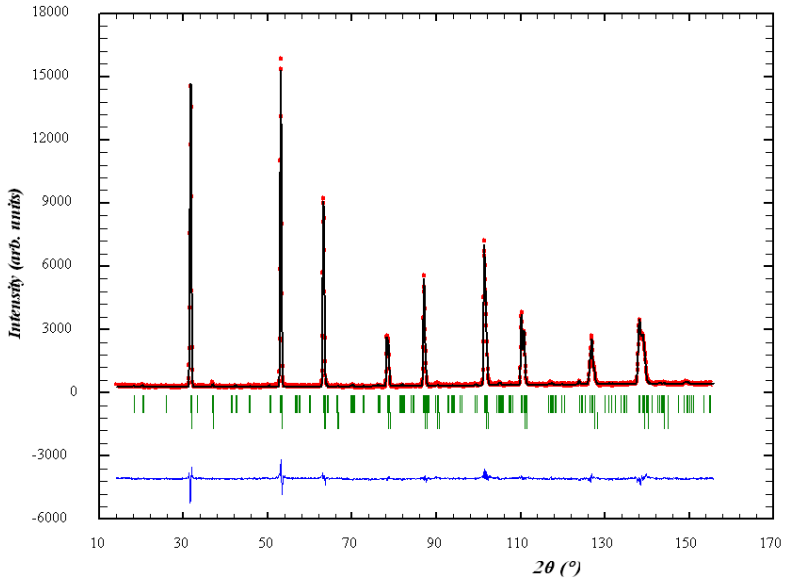

Kesterite-type

$Cu_2ZnSnSe_4$

E9, HZB

Germany

λ=1.7982 Å

Wurtz-Kesterite-type

$Cu_2ZnSiSe_4$

POWGEN, SNS

US

(ToF data)

G. Gurieva et al., J. Mat. Chem. A 14 (2026) 1770

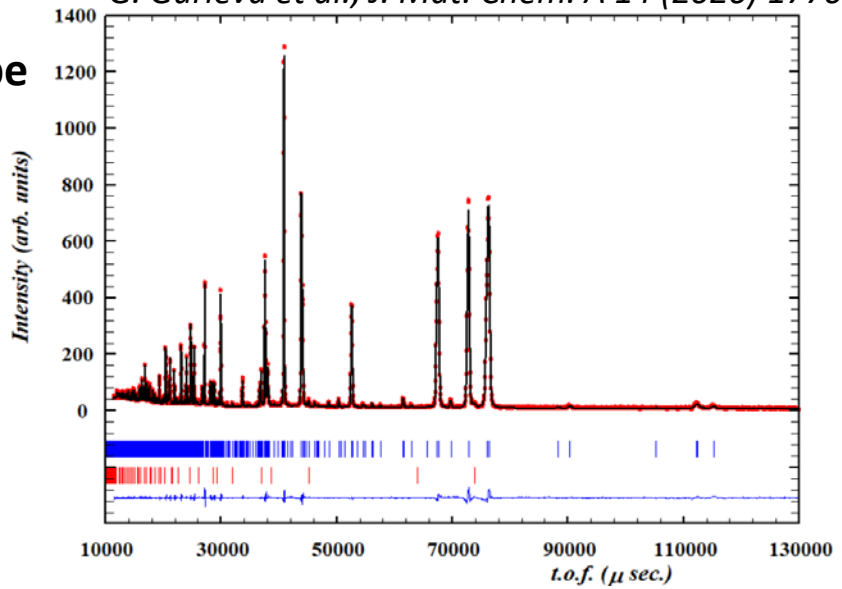

G. Gurieva et al., Faraday Discussions 239 (2022) 51

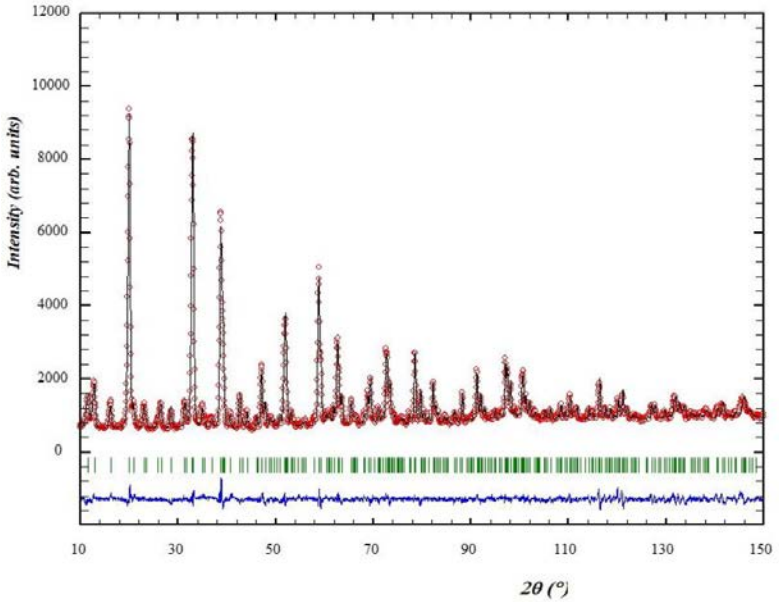

Stannite-type

$Cu_2MnSnSe_4$

HRPT, PSI

Switzerland

λ=1.1545 Å

Wurtz-Stannite-type

$Cu_2MnGeSe_4$

Echidna, ANSTO

Australia

λ=1.6215 Å

D. Matzdorff, PhD Thesis, FU Berlin, 2024

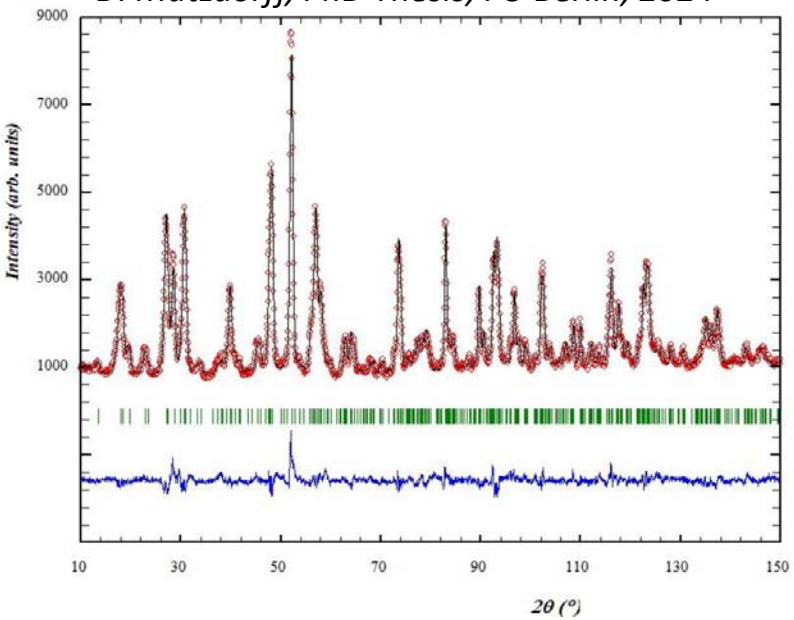

Ferroelectricity in $CH_3NH_3PbI_3$ ($MAPbI_3$)

- controversal discussion, publications are contradictive
- ferroelectric domains could explain strong light absorption of $MAPbI_3$

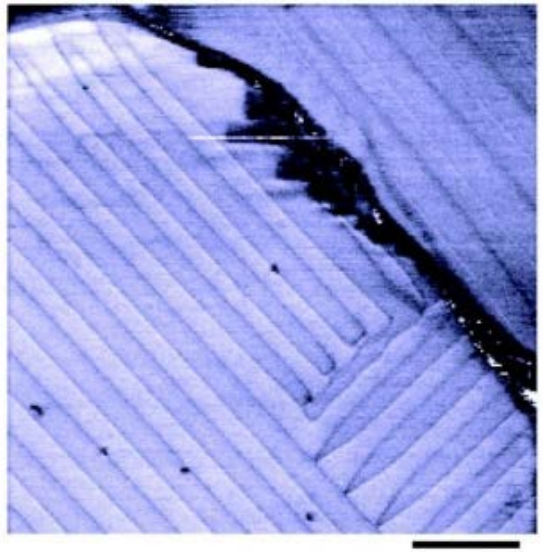

piezo-response force microscopy (PFM) in-phase image showing alternating polarized domains in $MAPbI_3$ thin-films

→ interpretation as polarized ferroelectric domains

H. Röhm et al., Energy Environ. Sci. 10 (2017) 950

(scale bar 360 nm)

pre-requesite for ferroelectricity → crystal structure without symmetry center

non-centrosymmetric space group

Centrosymmetry

- crystal class (point group) which contains an inversion center ($\bar{1}$) → **centrosymmetric**
- **crystals with an inversion center cannot display certain properties, such as piezoelectricity or, related to, ferroelectric properties**

- 21 crystal classes are non-centrosymmetric → 20 exhibit direct piezoelectricity (the 21st is the cubic class 432)

crystal system	centrosymmetric	non-centrosymmetric
triclinic	$\bar{1}$	1
monoclinic	$2/m$	$2, m$
orthorhombic	mmm	$222, mm2$
tetragonal	$4/m, 4/mmm$	$4, \bar{4}, 422, 4mm, \bar{4}m2$
trigonal	$\bar{3}m, \bar{3}m$	$3, 32, 3m$
hexagonal	$6/m, 6/mmm$	$6, \bar{6}, 622, 6mm, \bar{6}m2$
cubic	$m3, m\bar{3}m$	$23, \bar{4}3m, 432$

Can show ferrelectric properties!

Can $MAPbI_3$ be ferroelectric?

pre-requesite for ferroelectricity → crystal structure without symmetry center → **non-centrosymmetric space group**

BUT: $MAPbI_3$ crystallizes in the space group $I\frac{4}{m}cm$ (according to literature)
→ centrosymmetric space group → $MAPbI_3$ cannot be ferroelectric!

neutron diffraction on $MAPbI_3$ powder (neutron powder diffractometer @HZB)

in-depth analysis of the crystal structure → orientational disorder of the molecule breaks the inersion symmetry existing due to the symmetry $4 \perp m$ → **space group $I4cm$ → non-centrosymmetric space group!**

A. Franz, D. Toebbens and S. Schorr, Cryst. Res. Technol. 51 (9) (2016) 534–540

high resolution single crystal anomalous synX-ray diffraction on a $MAPbI_3$ single crystal
(beamline I19 at the synchrotron source Diamond/GB)

we showed that the MA molecule plays an important role as it distorts the neighboring iodide positions from their centrosymmetric positions

→ underlines the **mechanism of inversion symmetry breaking** (resulting in space group $I4cm$) → could explain ferroelectricity

J. Breternitz, S. Schorr et al., Angewandte Chemie Internat. Ed. 59 (2020) 424

atomic structure – external stimuli – stability

- nowadays the stability of hybrid halide perovskite based solar cells is limited to 1 year only
- for commercialisation a stability of 25 years is necessary

challenge → problems with long term stability of the halide perovskite absorber material

in-situ diffraction experiments with synchrotron X-rays

external stimuli **temperature, humidity and light** influence the atomic structure of halide perovskites

Impact of temperature

$FAPbBr_3$ (T=280-20K)

measured at KMC-2@BESSY II

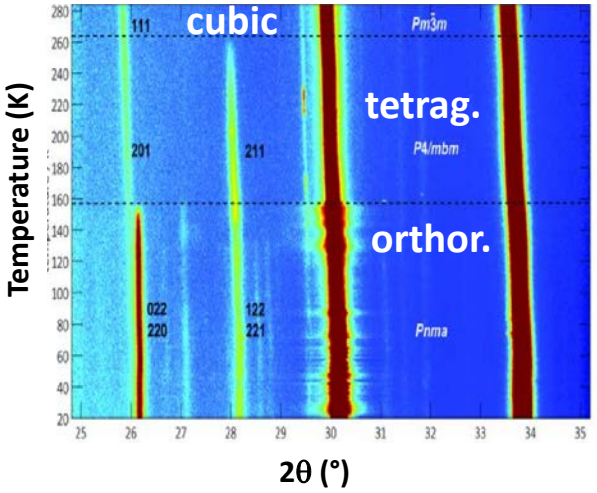

structural phase transitions

Franz, Schorr et al., Acta Cryst B 76 (2020) 267

$MAPb(I_{1-x}Br_x)_3$
T – x phase diagram

measured at KMC-2@BESSY II

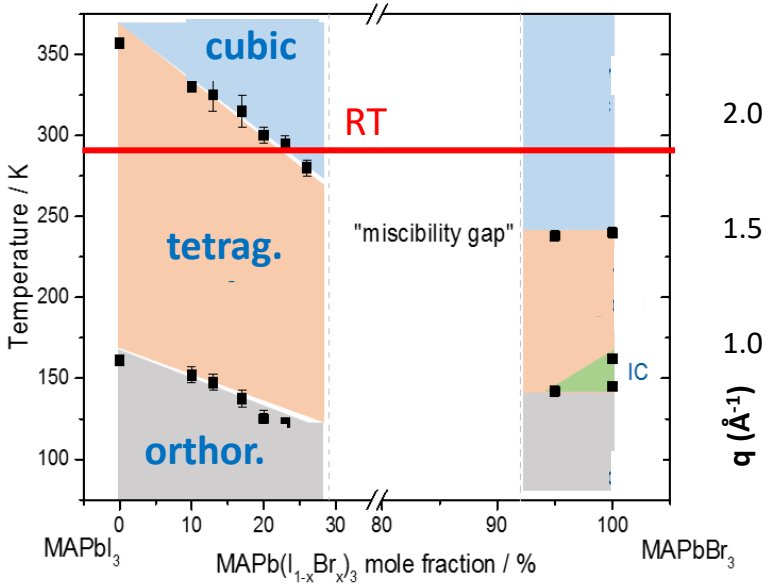

not a complete solid solution
→ broad miscibility gap

Lehmann, Schorr et al., RSC Adv. 9 (2019) 11151
Wiedemann, Schorr et al., J. Phys. Chem. Lett. 12 (2021) 2358

Impact of humidity

$(Cs,FA)PbI_3$ RH~100%

measured at NSLS

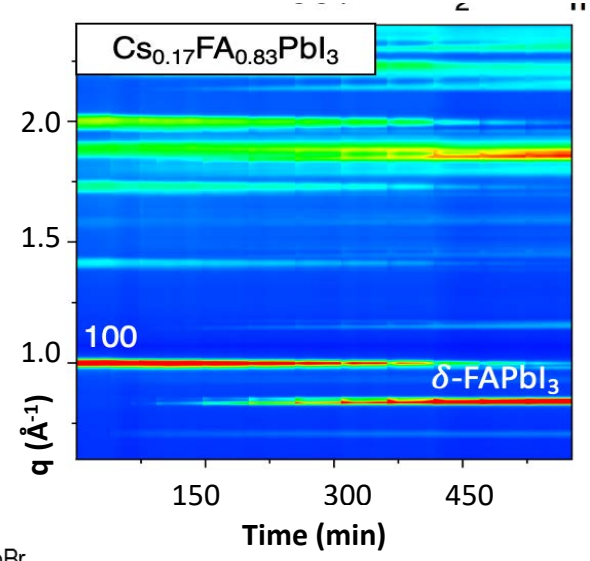

transformation from a cubic perovskit phase to a non-perovskite phase

Hidalgo, Schorr et al., J. Am. Chem. Soc. 145 (2023) 24549

Impact of light

$MAPbI_3$ light on/off

measured at MySpot@BESSY II (unpublished)

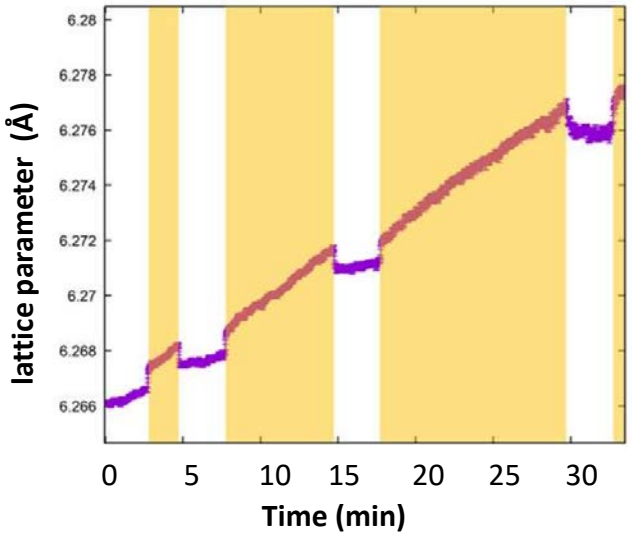

photoinduced lattice enhancement

Kim et al., Adv. OPt. Mat. 7 (2019) 1801512

Perovskite structure – network of corner sharing PbX_6 octahedra

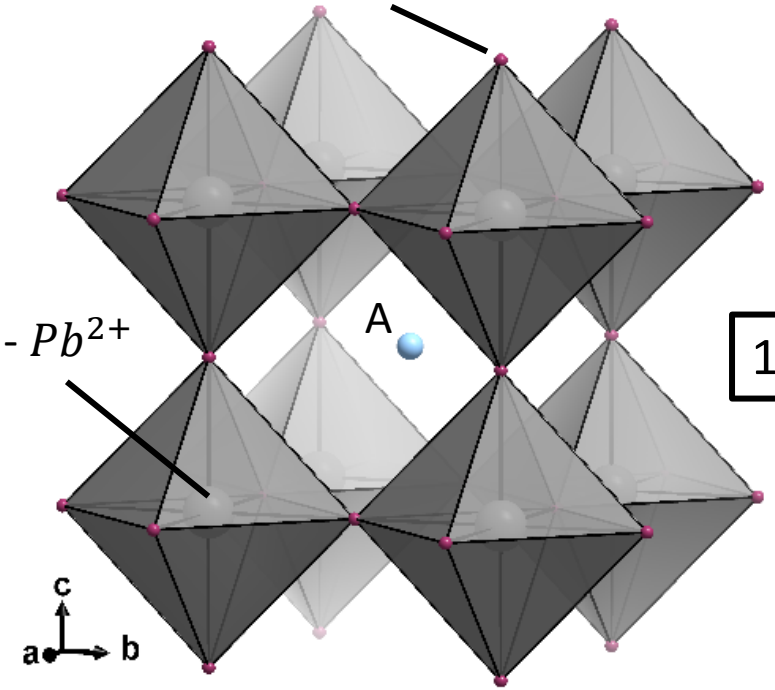

hybrid halide perovskite

all-inorganic halide perovskite

A - $[HC(NH_2)_2]^+$ (FA)
$[CH_3NH_3]^+$ (MA)

A … Cs^+

FA - Formamidinium
MA - Methylammonium

$MAPbI_3$

T > 330 K

cubic perovskite (α-phase)
(space group $Pm\bar{3}m$)

- complete orientational disorder of the molecule

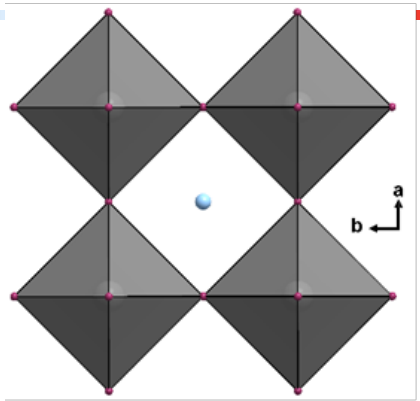

161 K < T < 330 K

tetragonal perovskite (β-phase)
(space group $I4cm$)

- orientational disorder of the molecule (e. g. 8 orientations in $MAPI_3$)
- tilting of the PbX_6 octahedra (distortet)

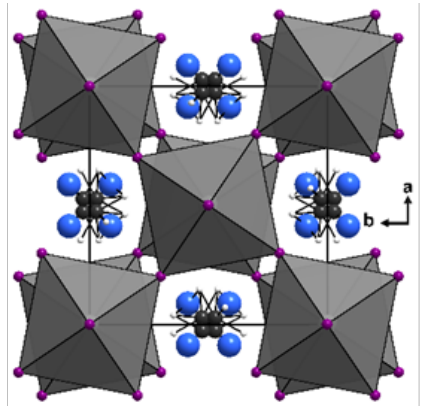

T < 161 K

orthorhombic perovskite (γ-phase)
(space group $Pnma$)

- orientational disorder of the molecule (e. g. 2 orientations in $MAPbCl_3$)
- tilting and kinking of the PbX_6 octahedra (distortet)

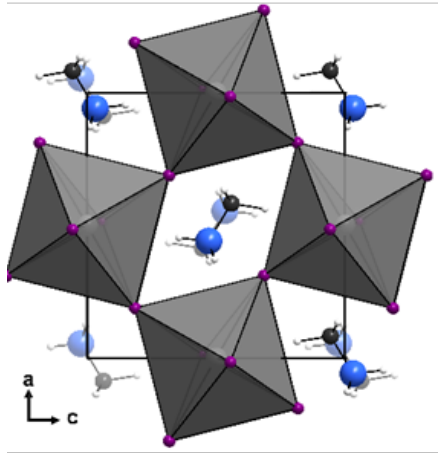

P. S. Whitfield et al., *Sci. Rep.* 6 (2016) 35685

Stabilization of the cubic phase in $FAPbI_3$

$FAPbI_3$ … lowest band gap energy (Eg~1.2 eV) amongst the hybrid halide perovskites

α-$FAPbI_3$

Perovskite
(cubic)

photoactive
(E_g~1.2 eV)

not stable at RT

2H-$FAPbI_3$

non-Perovskite
(hexagonal)

not photoactive

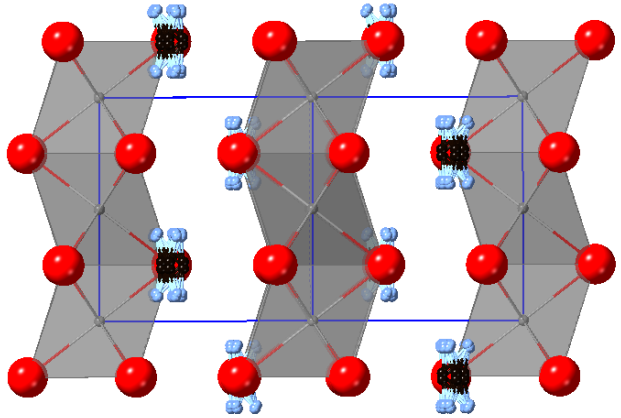

relatively stable at RT

optimized composition

- **to stabilize the cubic phase**
- **to reach high power conversion efficiency**

→ tiple-cation double anion perovskite*
$Cs_{0.05}(FA_{0.98}MA_{0.02})_{0.95}Pb(Br_{0.02}I_{0.98})_3$

**references*
G. Li et al., Science 379 (2023) 339
S. K. Tiwari, et al., IEEE J. Photovoltaics 13 (2023) 242
S. Mariotti et al., Science 381 (2023) 63

Low-T behavior of $Cs_{0.05}(FA_{0.98}MA_{0.02})_{0.95}Pb(Br_{0.02}I_{0.98})_3$

HZB Helmholtz Zentrum Berlin

in-situ X-ray diffraction @ BESSY II, KMC-2 beamline

cooling 300 K → 25 K

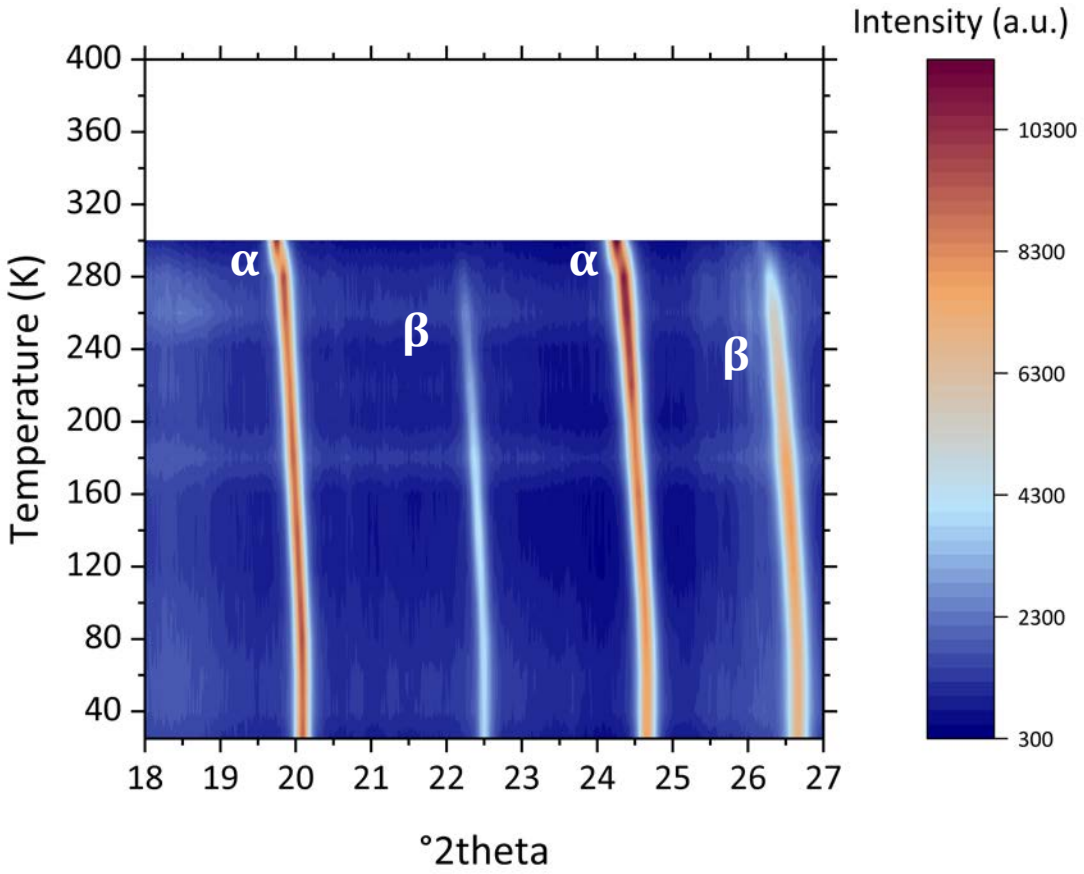

heating 25 K → 400 K

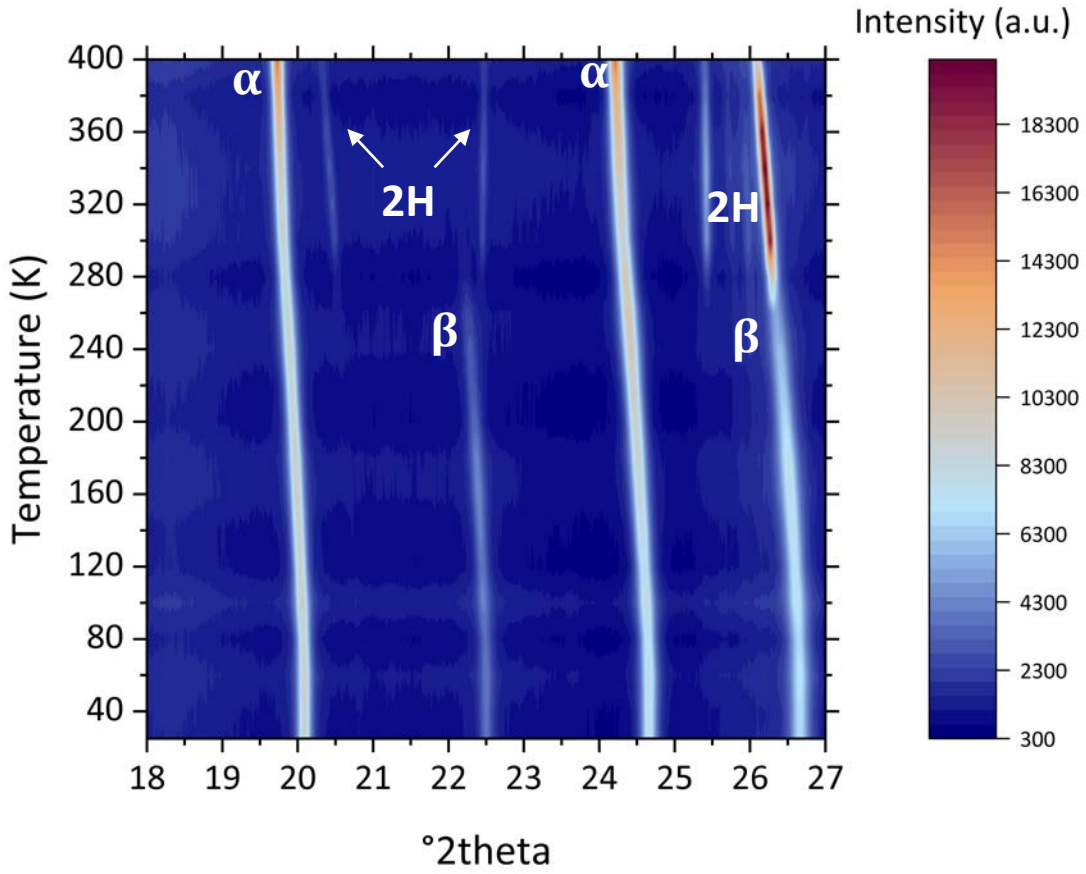

α → β at ~280 K

β → α at about ~300 K

Low-T behavior of $Cs_{0.05}(FA_{0.98}MA_{0.02})_{0.95}Pb(Br_{0.02}I_{0.98})_3$

HZB Helmholtz Zentrum Berlin

$Cs_{0.05}(FA_{0.98}MA_{0.02})_{0.95}Pb(Br_{0.02}I_{0.98})_3$

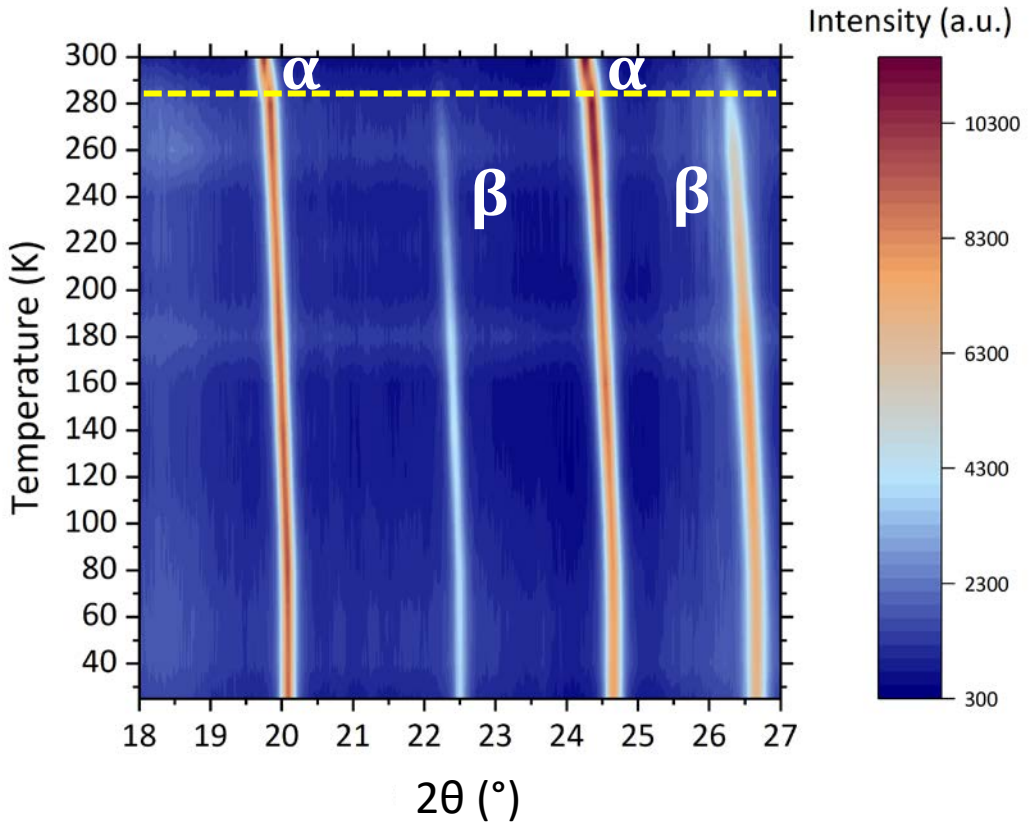

α → β phase transition at ≈280 K

no β → γ phase transition at low temperature

$Cs_{0.05}FA_{0.95}Pb(Br_xI_{1-x})_3$

Hidalgo, Schorr et al., Chem. Mater. 36 (2024) 10167

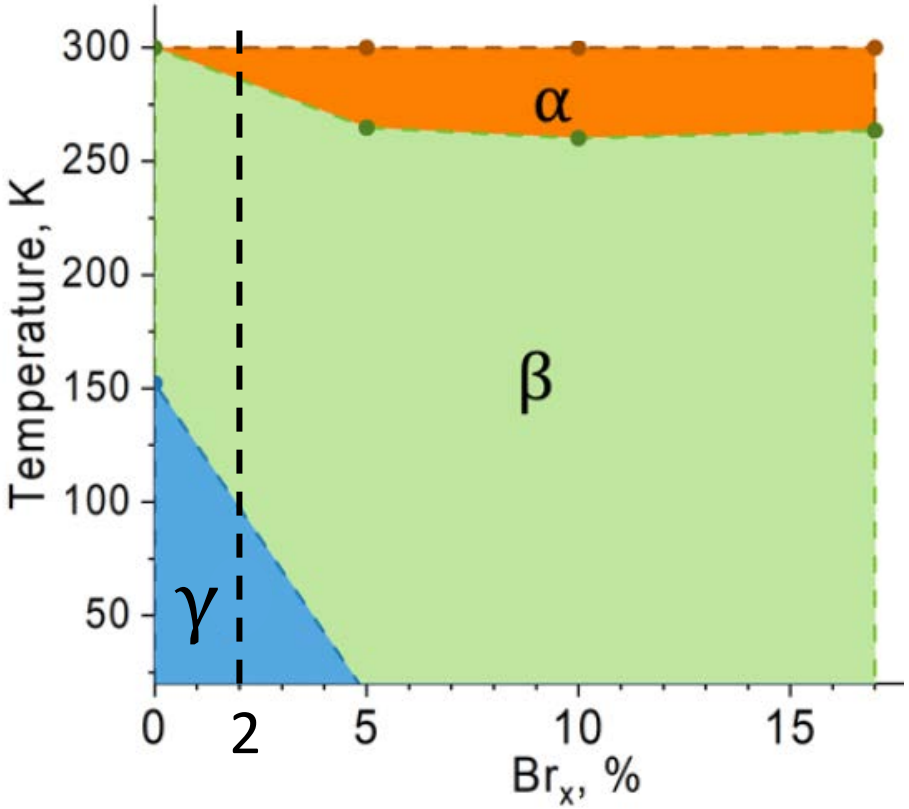

α → β phase transition at ≈280 K

β → γ phase transition at ≈100 K

substitution FA ↔ MA prevents the formation of the γ-phase in $Cs_{0.05}FA_{0.95}Pb(Br_{0.02}I_{0.98})_3$

Summary

understanding of
structure – property relations
of absorber materials
↓
absorber with optimized properties
↓
increase
efficiency
stability …
of thin films solar cells

developing
novel narrow and wide gap compound semiconductors
with
long term stabbility
abundant, non-toxic constituents
↓
new applications
tandem and triple junction thin film solar cells

in-depth investigation of the crystal structure of photovoltaic absorber materials (chalcogenides, halides) using neutrons and synchrotron radiation

↓

provides the basis for …

Acknowledgments

Thank you for your attention!

HZB Helmholtz Zentrum Berlin

my colleagues (*former*) from the Department Structure and Dynamics of Energy Materials at HZB

Dr. Galina Gurieva (quaternary chalcogenides)

Dr. Daniel Többens (KMC2-@BESSY II)

Dr. Ana Palacios-Saura (halide perovskites)

Dr. Joachim Breternitz (halide perovskites, ternary nitrides)

Dr. Dennis Wiedemann (halide perovskites)

Dr. Kai Neldner (CZTS)
Dr. Elisa Valle-Rios (CZTSe)
Dr. Rene Gunder (CZGeSe)
Dr. David Matzdorff (Mn-comp.)
Dr. Frederike Lehmann (FA/MAPI/Br)
Dr. Zhenyu Wang ($ZnGeN_2$)

} former PhD students

instrument scientists (neutron diffraction) at **neutron sources** all over the world

- former BERII at HZB, Germany
- Institute Laue-Langevin (ILL), Grenoble, France
- Paul-Scherrer-Institute (PSI), Villigen, Switzerland
- SNS, Oak Ridge National Lab, US
- ANSTO, Lucas Heights (near Sydney), Australia

instrument scientists (synX-ray diffraction) at **synchrotron radiation sources**

- ESRF, Grenoble, France
- Diamond Light Source, UK

KESTCELLS (2012-2015)

STARCELL (2017-2019)

INFINITE CELL (2018-2023)

CUSTOM-ART DISRUPTIVE KESTERITE-BASED (2020-2023)

ReNewPV (2024-2026)

INDIGO (2027-2029)

Cooperation partners (just a selection)

UNIVERSITÄT LEIPZIG

MARTIN-LUTHER-UNIVERSITÄT HALLE-WITTENBERG

UNIVERSITÉ DU LUXEMBOURG

IREC Institut de Recerca en Energia de Catalunya Catalonia Institute for Energy Research

UAM UNIVERSIDAD AUTONOMA DE MADRID

Imperial College London

TAL TECH

crystalsol

PVICOKEST **International Cooperative Programme for Photovoltaic Kesterite Based Technologies** (FP7-PEOPLE-2010-IRSES)

KESTCELLS **Training for sustainable low cost PV technologies: development of kesterite based efficient solar cells** (FP7-PEOPLE-2012-ITN)

STARCELL **Innovative and sustainable materials solutions for the substitution of critical raw materials (CRM) in the electric power systems, in particular CRM in materials used in photovoltaic cells** (H2020-NMBP03-2016-720907)

INFINITE CELL **International cooperation for the development of cost-efficient kesterite/c-Si thin film next generation tandem solar cells** (H2020-MSCA-RISE-2017-777968)

CUSTOM-ART DISRUPTIVE KESTERITE-BASED **Disruptive kesterite-based thin film technologies customized for challenging architectural and active urban furniture applications** (H2020-LC-SC3-2018-2019-2020)

Neutron scattering length *b*

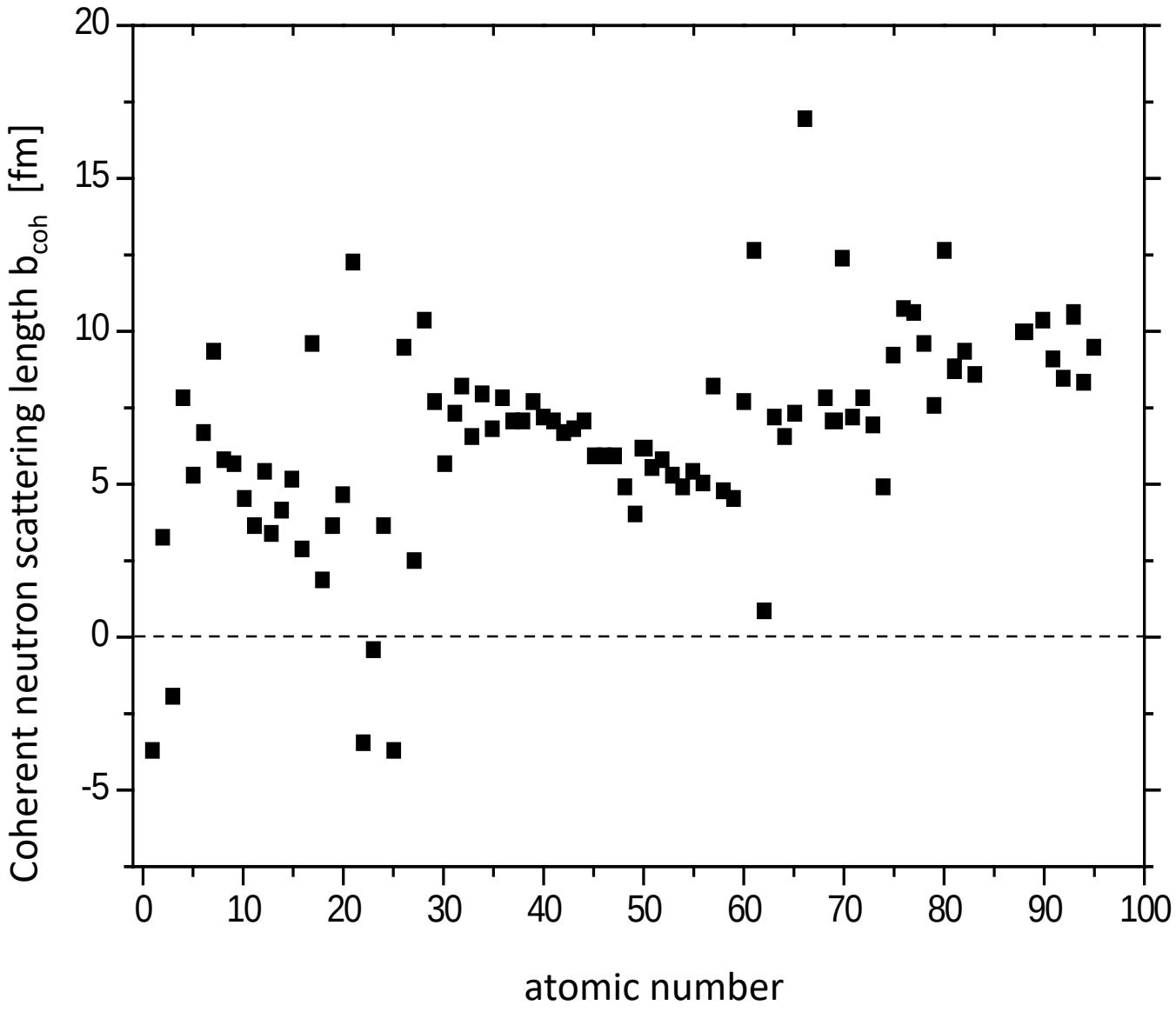

- *b* corresponds to the form factor in X-ray scattering
- *b* is independent of the neutron energy
- *b* has units of length ~10^{-12} cm
- *b* varies randomly with Z and isotope

→ allows access to atoms that are usually unseen by X-rays

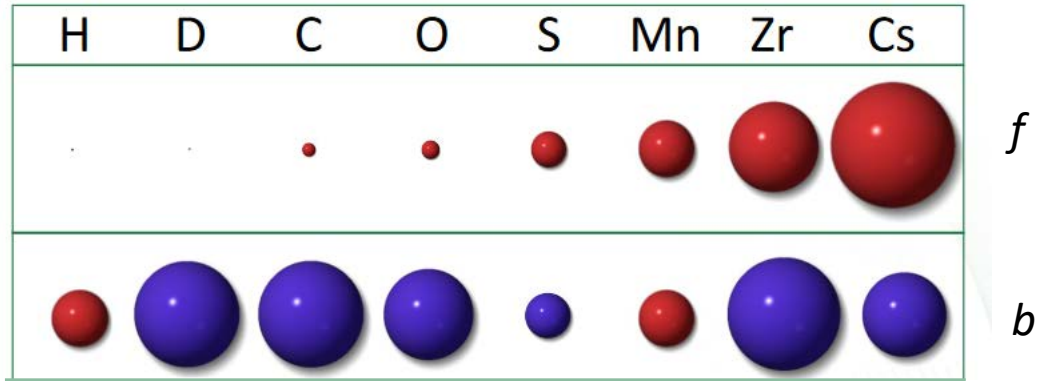

Average neutron scattering analysis method

cation site occupancies (SOF)

from Rietveld analysis of

neutron diffraction data

neutron scattering lengths

Cu: 7.718 fm

Zn: 5.680 fm

Sn: 6.225 fm

Ge: 8.185 fm

experimental average neutron scattering length

$$\bar{b}_{2a}(\text{exp}) = SOF_{2a} \cdot b_{Cu}$$
$$\bar{b}_{2c}(\text{exp}) = SOF_{2c} \cdot b_{Cu}$$
$$\bar{b}_{2d}(\text{exp}) = SOF_{2d} \cdot b_{Zn}$$
$$\bar{b}_{2b}(\text{exp}) = SOF_{2b} \cdot b_{IV}$$

calculated average neutron scattering length → cation distribution model based on off-stoichiometry types

$$\bar{b}_j(calc) = \sum_k (k)_j^{model} \cdot b_k$$

j=2a, 2c, 2d, 2b
k=Cu,Zn, IV

$(k)_j^{model}$ *- fraction of cation k on site j*

additional requirements:

(1) each cation site is fully occupied

$$(k)_j^{model} + V_j^{model} = 1$$

j=2a, 2c, 2d, 2b
k=Cu,Zn,IV (Sn,Ge)
V - vacancy

(2) the sum of a cation species in the model is the cation species amount measured by WDX

$$\sum_j (k)^{model} = k^{WDX}$$

Schorr et al. in: Advanced characterization techniques for thin film solar cells, Wiley, 2016

Defect tolerance

HZB Helmholtz Zentrum Berlin

defect tolerant semiconductors

- tendency of a semiconductor to keep its properties despite the presence of crystallographic defects
- high light conversion efficiency is maintained despite high concentration of point defects

Defect tolerance can be arised by

(i) Point defects can form **defect pairs** → electronically beinign complexes
example: chalcopyrites like $Cu(In,Ga)Se_2$

Zhang, Wei, Zunger, Phys. Rev. B 57 (1998) 9642

comprehensive study of point defects in chalcopyrites by neutron diffraction

- *Stephan, Schorr, Schock, APL 98 (2011) 091906*
- *Stephan et al., APL 101 (2012) 101907*
- *Stephan et al., J. Phys. Chem. Sol. 98 (2016) 309*

(ii) point defects can be less harmfull if dominant traps within the band gap are energetically **close to valence or conduction band edges** (shallow)

(iii) point defects can be less harmfull if they have **low capture cross sections**

found for hybrid metal halide perovskites

↓

important factor behind the rapid increase of device efficiency

A.M. Genose et al., Nature Communication 13 (2022) 4715

Overcoming Shockley-Queisser limit: tandem solar cell

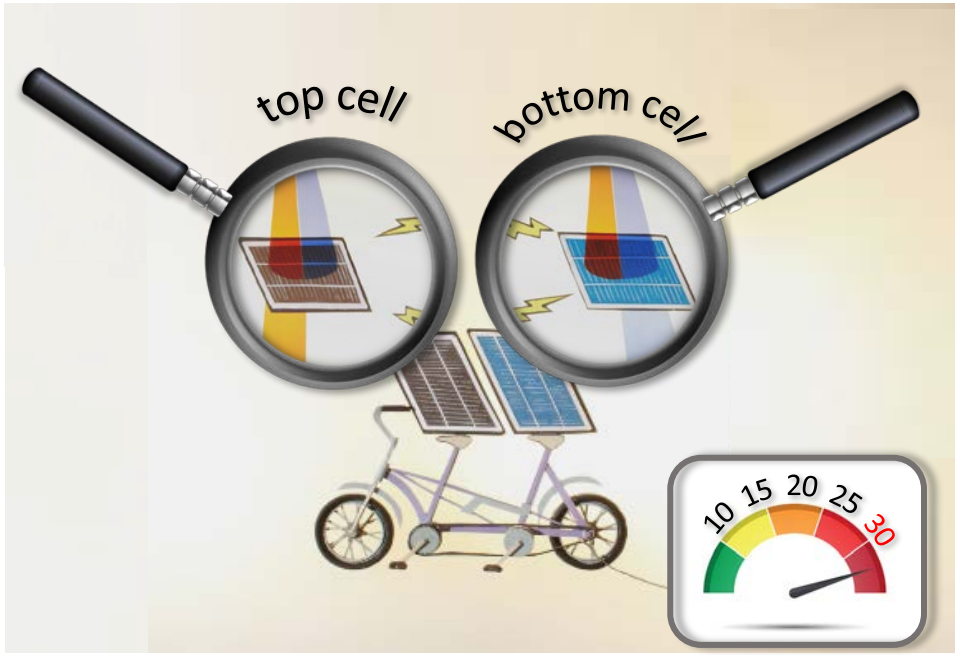

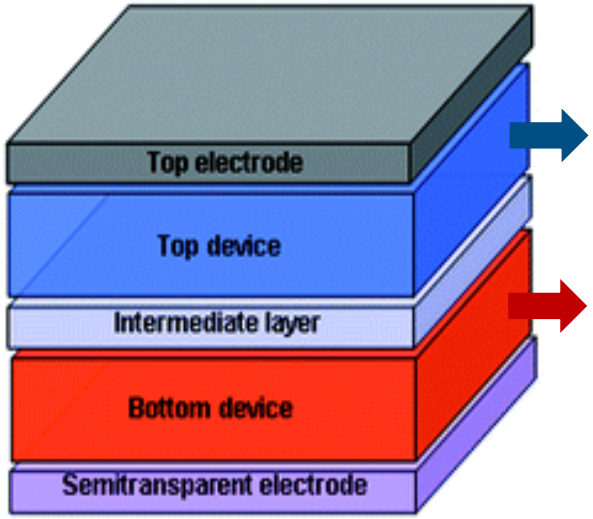

Multi-junction solar cell

wide band gap semiconductor

narrow band gap semiconductor

Ameri et al., Energy Environ. Sci. 2 (2009) 347–363

Maximum efficiency for a band gap value as part of a multi-junction stack

Bremner et al., Solar Energy 135 (2016) 750.

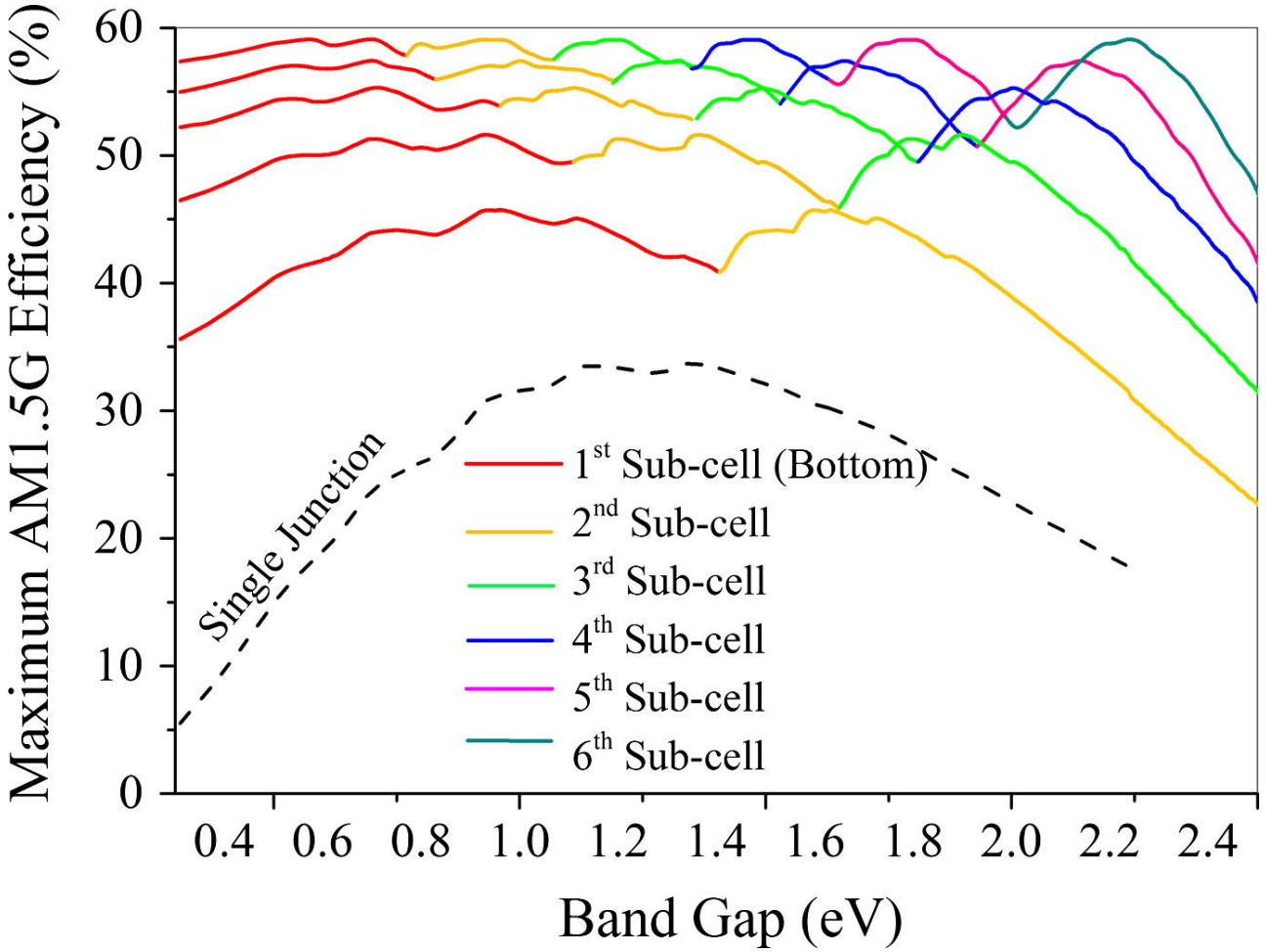

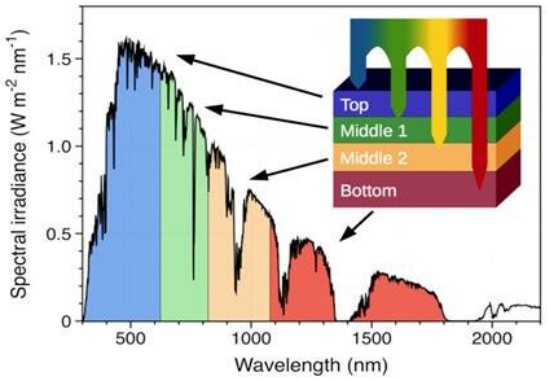

multi-junction device

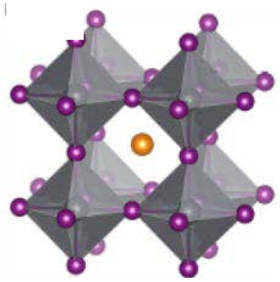

perovskites
network of corner sharing octahedra

ABX_3 compounds

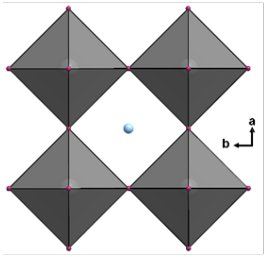

cubic perovskite
(space group $Pm\bar{3}m$)
e. g. $MAPbBr_3$

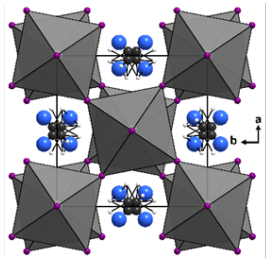

tetragonal perovskite
(space group $I\frac{4}{m}cm$)
e. g. $MAPbI_3$

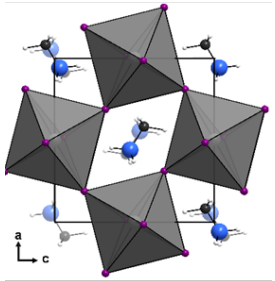

orthorhombic perovskite
(space group $Pnma$)
e. g. $MAPbCl_3$

increasing distortion of the coordination polyhedra

adamantines
network of corner sharing tetrahedra

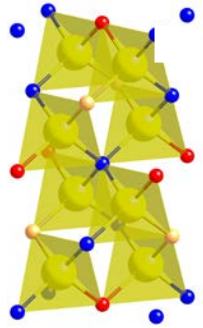

A_2BCX_4 compounds

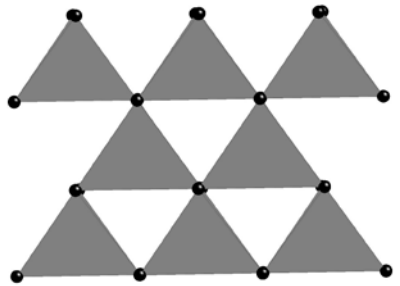

tetragonal stannite
(space group $I42m$)
e. g. Cu_2MnSnS_4

tetragonal kesterite
(space group $I4$)
e. g. $Cu_2ZnGeSe_4$

orthorhombic wurtz-stannite
(space group $Pnm2_1$)
e. g. Cu_2MnGeS_4

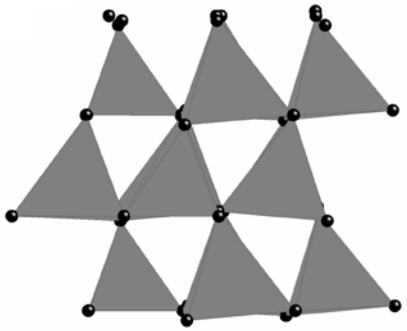

monoclinic wurtz-kesterite
(space group Pn)
e. g. $Cu_2ZnSiSe_4$

Orientational disorder of the molecule MA^+ in $MAPbI_3$

X-ray powder diffraction
@KMC-2 (BESSYII)

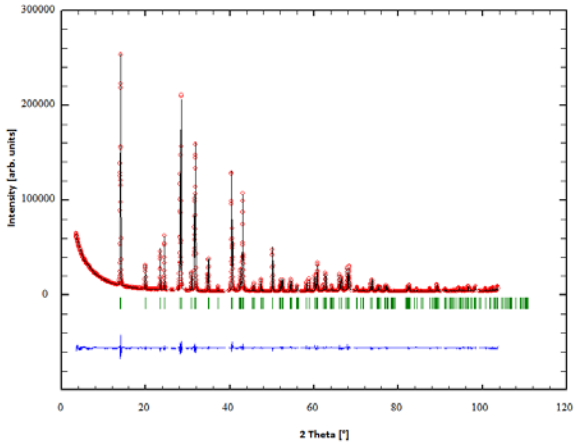

neutron powder diffraction
@E9 (BERII)

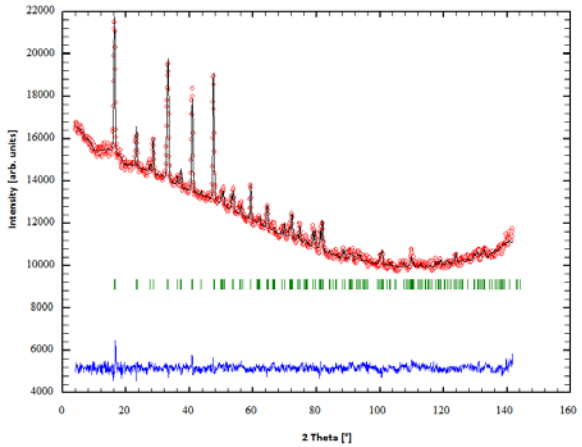

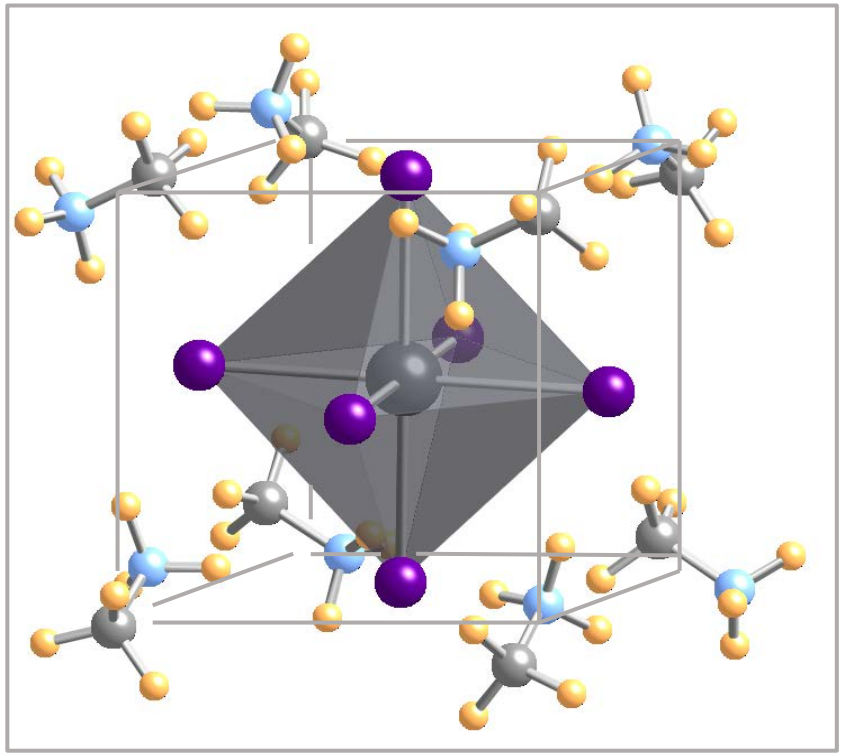

- perovskite (space group $I4cm$ → non-centrosymmetric)
- MA^+ molecules are aligned in <221>
  → 8 possible orientations → **8-fold disordering**
- PbI_6 octaedra tilting occurs along [001]
  → tilts allow the iodide ions to move towards the $-NH_3$ end of molecule
  → thereby satisfying the coordination preferences of both polar and non-polar ends of the molecules
- reasonable strong hydrogen bonded NH – I distances (2.687 Å, compare 2.598 Å in NH_4I)

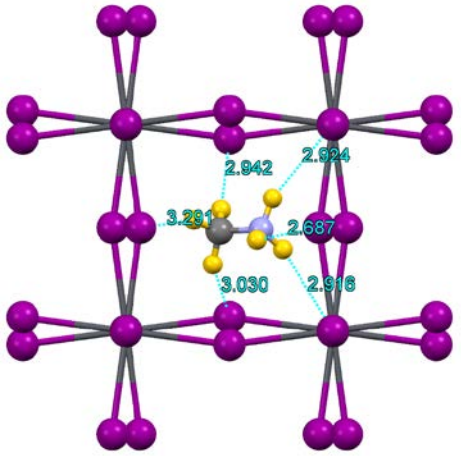

Franz, Schorr et al., Cryst.Res.Technol. 51 (2016) 534

rotational dynamics of $(CH_3NH_3)^+$ (MA) ions in $MAPbI_3$

4-fold rotations of the molecule

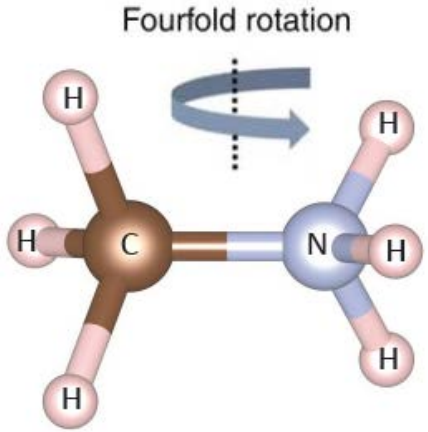

3-fold rotations of the molecule

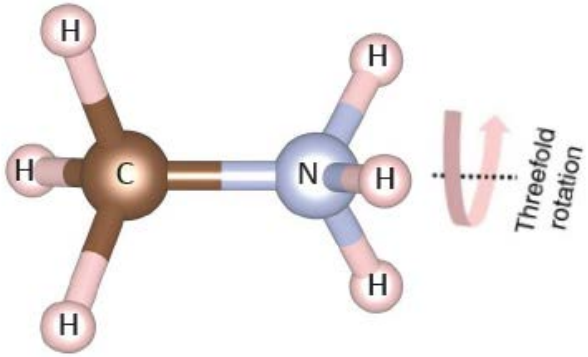

*Chen et al., Phys.Chem.Chem.Phys., **17** (2015) 31278*

MAPI in the tetragonal phase (161 K – 327 K)

$I4cm$*

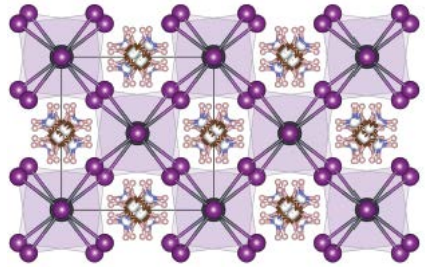

- structural disorder of the MA molecule, 8 different orientations *
  - $(CH_3NH_3)^+$ ions exhibit a 4-fold rotational symmetry of the C – N axis (C_4) along with a 3-fold jump rotation along the C – N axis (C_3)

  → $C_3 \otimes C_4$ model
  - the $C_3 \otimes C_4$ model includes
    - one elastic component
    - 5 quasi-elastic components

MAPI in the orthorhombic phase (T<161 K)

$Pnma$

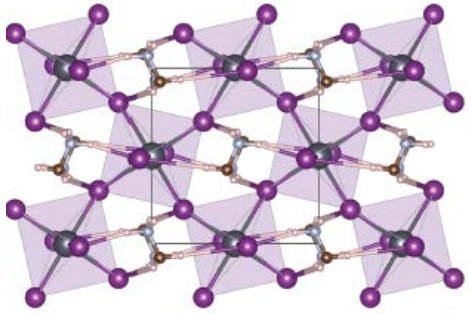

- only 2 different orientations of the MA molecule
- only C_3 jump rotations of the $(CH_3NH_3)^+$ ions are present (rotational jump model C_3)

**A. Franz et al., Cryst.Res.Technol. 51 (2016) 534*

Influence of chlorine on the hydrogen-halide bonding in halide perovskites

FTIR investigations* indicate → **in the orthorhombic phase (T < 161 K) the iodide is more strongly influenced by hydrogen bonding than the chloride**

QENS data of $MAPbI_3$, $MAPbCl_3$ and $MAPb(I,Cl)_3$ T=70K

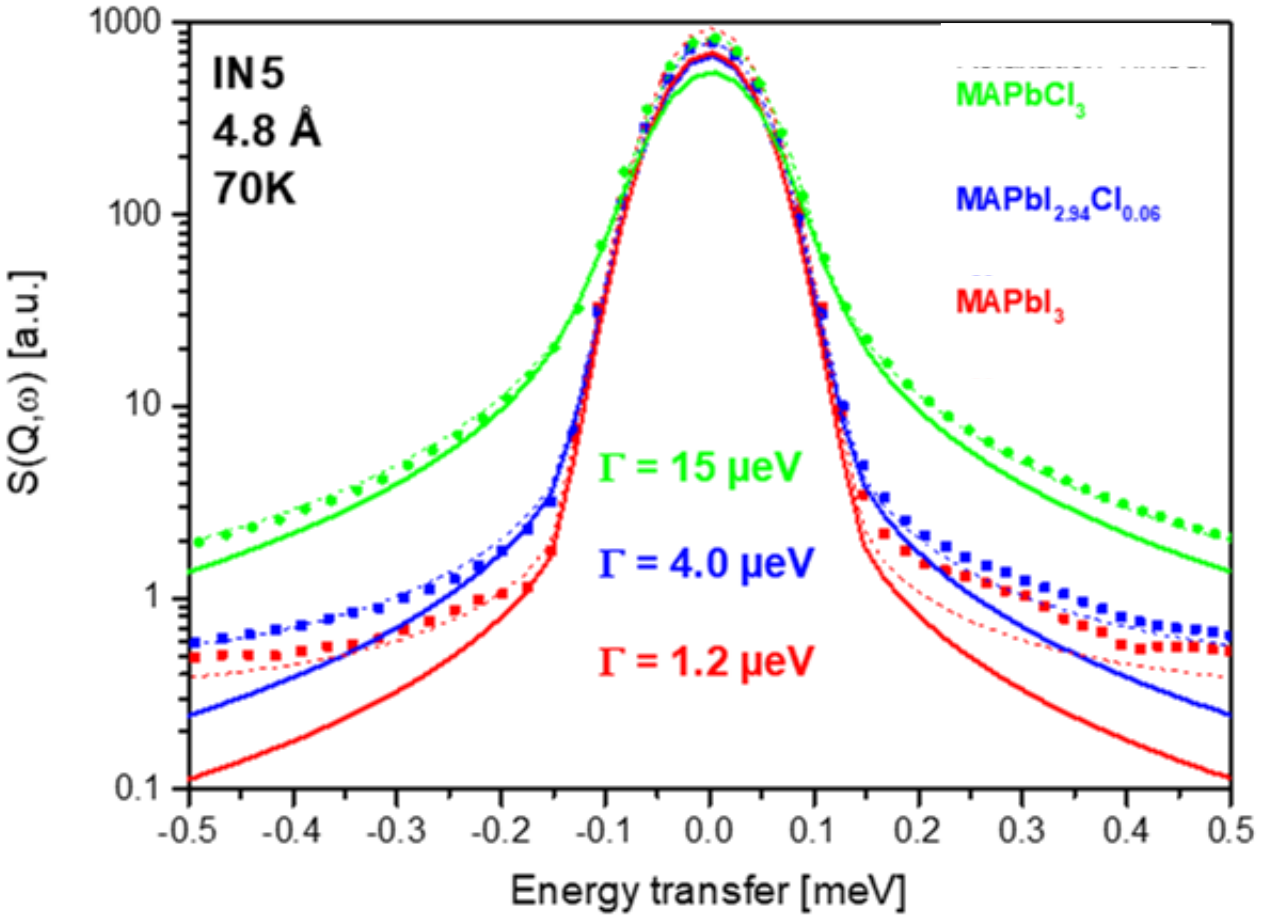

MA molecule in cuboctahedral coordination by the halide

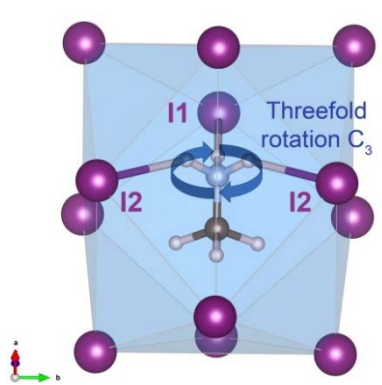

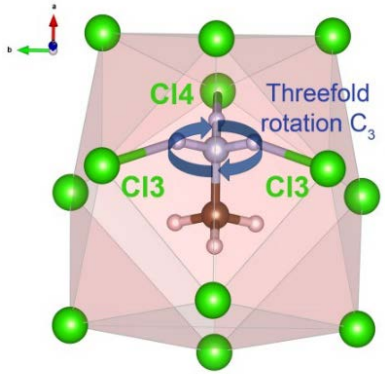

characteristic relaxation time τ of the C_3 jump rotation

$$\Gamma_{C3}[meV] = \frac{3\hbar}{\tau_{C3}[ps]}$$

1635 ps > 485 ps > 135 ps

Chlorine substitution in MAPI (orthorhombic phase)
→ leads to a weakening of the hydrogen bonds

G. Schuck, D. M. Többens, M. Koch-Müller, I. Efthimiopoulos, and S. Schorr, J. Phys. Chem. C 122 (2018) 5227

G. Schuck et al., J. Phys. Chem. C 123 (2019) 11436

Activation energies: $MAPI_3$, $MAPbI_{2.94}Cl_{0.06}$ and $MAPbCl_3$

Temperature dependent behaviour of Γ_{C3}

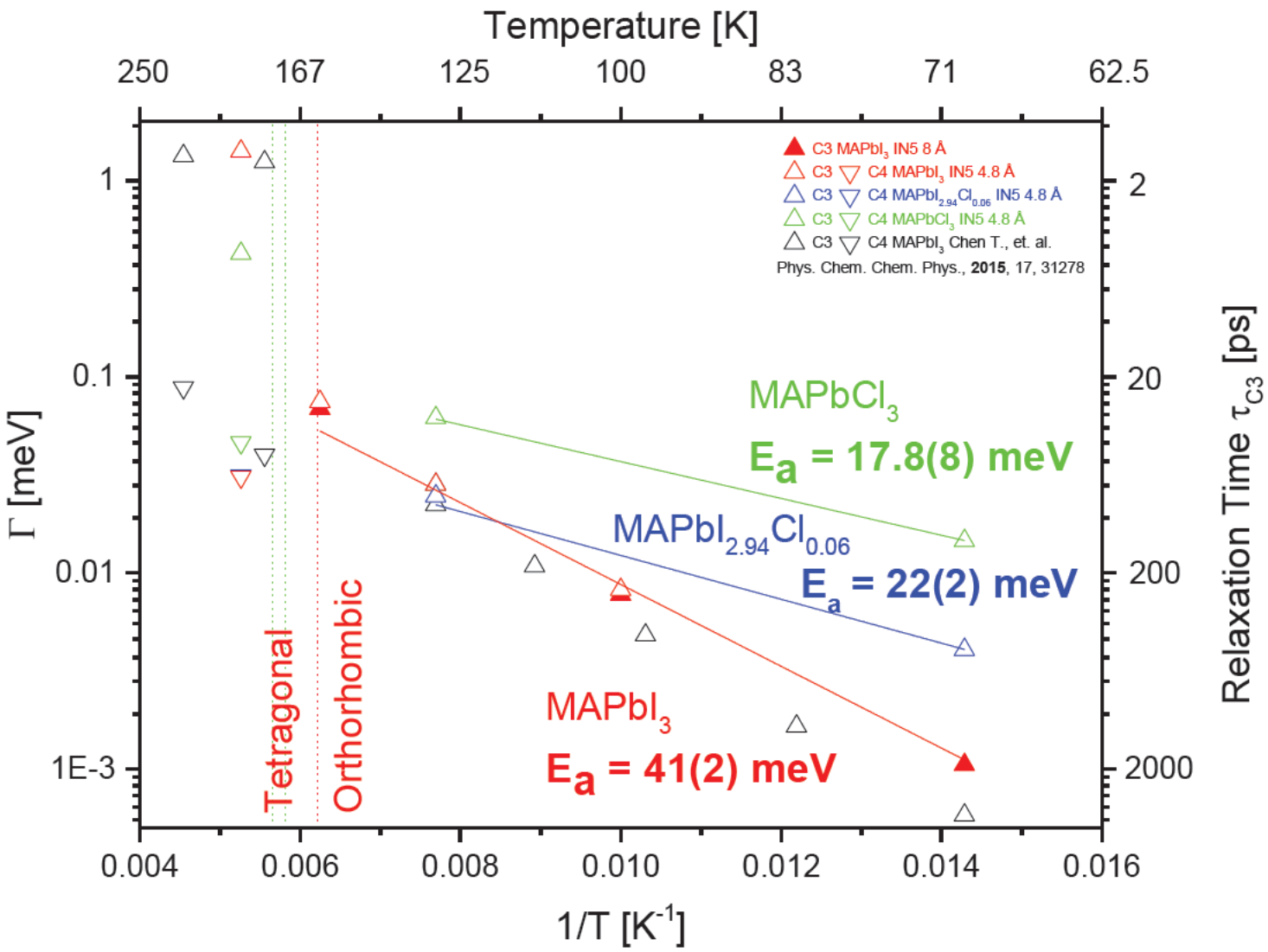

Activation energy E_a

$$\ln(\tau) = \frac{E_a}{k_B T} - \ln(A)$$

k_B: Boltzmann constant
A: pre-exponential factor

- E_a for to **$MAPbI_3$** in the range of literature data (Chen et. al. 2015)
- significant decrease of E_a in **$MAPbI_{2.94}Cl_{0.06}$** and **$MAPbCl_3$** compared to **$MAPbI_3$**

E_a indicates that chlorine substitution leads to a weakening of the hydrogen bridge bonds

*Chen et al., Phys.Chem.Chem.Phys., **17** (2015) 31278*

G. Schuck, S. Schorr et al., J. Phys. Chem. C 123 (2019) 11436